

Geochemical and Petrological Insights into the Neoproterozoic Moumba Metabasites: Implications for Crustal Processes in the West Congo Belt (Republic of Congo)

Ulrich Verne Matiaba-Bazika^{1,2*}, Nelson Lekeba Makamba^{1,2},
Vicky Tendresse Télange Bouénitéla¹, Nicy Carmelle Bazebizonza Tchiguina^{1,3},
Timothée Miyouna¹, Florent Boudzoumou^{1,2}

¹Laboratory of Geosciences, Faculty of Sciences and Technics, Marien NGOUABI University, Brazzaville, Republic of Congo

²National Institute for Research in Exact and Natural Sciences (IRSEN), Brazzaville, Republic of Congo

³Geographid Research and Cartographic Production Center (CERGEC), Brazzaville, Republic of Congo

Email: *iletbazika@gmail.com, nelsonlekebamakamba@gmail.com, Vicky_bouenitela@yahoo.fr, nicybazebizonza@gmail.com, miyounatim@yahoo.fr, boudzoumouf@gmail.com

How to cite this paper: Matiaba-Bazika, U. V., Lekeba Makamba, N., Bouénitéla, V. T. T., Tchiguina, N. C. B., Miyouna, T., & Boudzoumou, F. (2024). Geochemical and Petrological Insights into the Neoproterozoic Moumba Metabasites: Implications for Crustal Processes in the West Congo Belt (Republic of Congo). *Journal of Geoscience and Environment Protection*, 12, 1-29. <https://doi.org/10.4236/gep.2024.122001>

Received: October 5, 2023

Accepted: January 10, 2024

Published: February 7, 2024

Copyright © 2024 by author(s) and Scientific Research Publishing Inc. This work is licensed under the Creative Commons Attribution International License (CC BY 4.0).

<http://creativecommons.org/licenses/by/4.0/>



Open Access

Abstract

The West Congo Belt contains in its rocks of Neoproterozoic age from Nemba complex outcropping in the Moumba River. This West Congo belt is made up of a crustal segment of the Arcaui-West Congo orogen which extends from southwest Gabon to the northeast of Angola. This study aims to constrain the geochemical signature Nemba complex of West Congo belt from the petrographic and geochemical study on the whole rock. The petrographic data from this study show the Moumba metabasites are made up of amphibolites, metagabbros, epidotites and greenschists interstratified in the Eburnean metasediments and affected by mesozonal to epizonal metamorphism characterized by the retromorphosis of intermediate amphibolite facies minerals into greenschist facies. Whole-rock geochemical data indicate that these metabasites are continental flood basalts (CFB) of basic nature and transitional affinity emplaced in intraplate context. These continental flood basalts are generated from magma originating from a significantly enriched shallow mantle plume and this magma then contaminated by the continental crust during their ascent. The reconstruction of tectonic signature suggests that West Congo belt would result from closure of an ocean basin with subduction phenomena. This collision would be marked by the establishment of ophiolite complex. We show that this model is incompatible with the CFB nature of metabasites and the orogenic evolution of Neoproterozoic. It does not seem that we can evoke a genetic link with a subduction of oceanic crust, because

the paleogeography of Neoproterozoic (Rodinia) is marked by intracontinental rifts linked to opening of Rodinia. We therefore suggest the non-existence of ophiolitic complex in western Congo belt and reject the collisional model published by certain authors. We confirm the currently available intracontinental orogen model.

Keywords

Mayombe, Metabasites, Moumba, Mantle Plume, Continental Rifting, Basalts Flood Continental

1. Introduction

The West Congo belt is a pan-African mobile belt located in the western part of central Africa. This belt is part of a segment of the Araçuaí-Congo orogen (Teixeira & Figueiredo 1991; Heilbron & Machado 2003; Pedrosa-Soares et al., 2008; Pedrosa-Soares et al., 2011), which extends parallel to the Atlantic coast from southwest Gabon to northeast Angola over 1400 km long and 100 to 150 km wide (Dadet, 1969; Maurin, 1993). It consists of a juvenile Neoproterozoic continental crust formed during the Pan-African orogeny, with a heritage of older Paleoproterozoic crustal rocks (Dadet, 1969; Hossie, 1980; Boudzoumou, 1986; Maurin, 1993). This belt comprises igneous and metamorphic rocks, as well as green rocks affected by two phases of deformation (Boudzoumou, 1986). Metabasites of the Neoproterozoic age of Mayombe belt crop out in intermediate domain. This domain consists of formations from the lower part of the Western Congo Supergroup (Fullgraf et al., 2015). It contains basic siliciclastic rocks, volcanoclastic rocks and metasediments (Fullgraf et al., 2015). The metabasites subject of this study represents a large formation called the Nemba Complex (Fullgraf et al., 2015).

The study area is located in the northwest part of the Mayombe Belt, consisting of metasediments and metabasites attributed to the Nemba Complex (Bazika et al., 2022). This study focuses only on the metabasites rocks outcropping in the Moumba River.

The origin and geodynamic setting of the Araçuaí-West Congo Orogen (AWCO) have been the subject of numerous controversies both on the African margin and the Brazilian margin, linked to various geodynamic staging contexts: 1) Vellutini et al. (1983) and Vicat & Vellutini (1987) interpret these metabasites as ophiolitic basalts, resulting from the ocean closure with subduction phenomena. This hypothesis is supported in the Brazilian margin by Pedrosa-Soares et al. (1998) and Alkmim et al. (2006) who suggest the existence of oceanic crust in the Macaúbas Basin. Pedrosa-Soares et al. (2000) and Pedrosa-Soares et al. (2008) interpret the metabasites of the Macaúbas Group in the Araçuaí belt as an ophiolitic remnants, related to a wrench tectonics in a subduction setting; 2) Tack et al. (2001); Fullgraf et al. (2015); Djama et al. (2018) and Bazika et al. (2022) re-

ject this interpretation and consider them as intraplate basalts. Fullgraf et al. (2015) and Djama et al. (2018) suggest that these metabasites are part of intraplate basalts linked to the opening of Rodinia. Tack et al. (2001) and Bazika et al. (2022) interpret these metabasites as trap basalts (CFB) due to crustal extension. In the Brazilian margin, Cavalcante et al. (2019) also consider the metabasites of the Macaúbas Group in the Araçuaí belt as intraplate basalts. Despite the rifting episode presented by these two hypotheses, neither of them makes it possible to convincingly integrate all the petrographic and geochemical data of all the Neoproterozoic metabasites of this orogen. As a result, several questions remain: what are the nature, origin and exact geodynamic context of the metabasites of the Araçuaí-West Congo orogen? It is with the perspective of answering this question that we undertook to constrain the nature, origin, and geodynamic context of the Nemba complex of the West Congo belt from the petrographic and geochemical study of the metabasites of Moumba.

2. Geological Overview

The Araçuaí-West Congo Orogeny resulted from the collision between the Sao Francisco craton and the Congo craton (Figure 1(A), Figure 1(B)). It amalgamated during the late stages of the Neoproterozoic (Tack et al., 2001; Noce et al., 2007; Nsungani, 2012; Affaton et al., 2016).

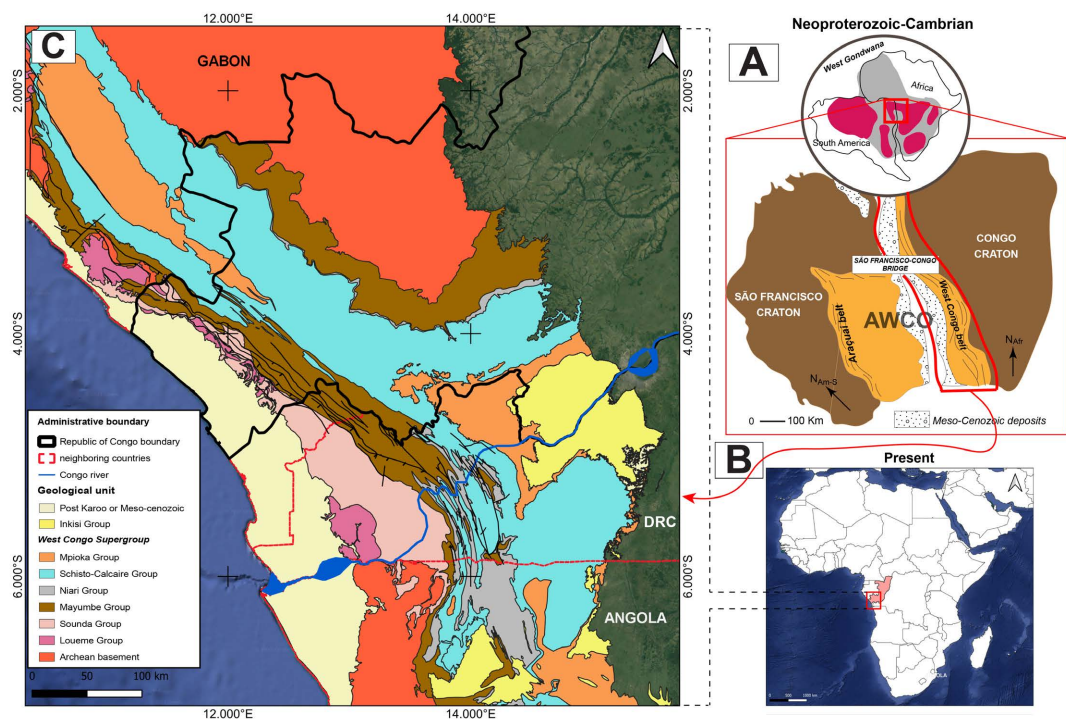


Figure 1. Geological context of the study area: A. Geological map of Archean to Phanerozoic formations in the western part of Central Africa (modified from Maurin et al. (1991); Affaton et al. (2016) and Le Bayon et al. (2015)); B. Geological map of the Araçuaí-West Congo system showing a portion of the western Gondwana outlining the AWACO system (modified from Pedrosa-Soares et al., 2011). Simplified geological map of the West Congo Orogen.

The West Congolian belt is constitutes a prominent topography with an NNE orientation consistent with the initial structural trend of the belt (Hossie, 1980; Boudzoumou, 1986; Djama, 1988; Maurin, 1993; Vicat & Pouclet 2000; Tack et al., 2001; Frimmel et al., 2011, Thiéblemont et al., 2018) (Figure 1(C)). This high domain generally measures less than 200 km and is followed to the east by a low and flat domain, known as the Niari-Nyanga Basin in Gabon and Congo, where it is bordered to the northeast by the basement of the Ntem-Chaillu block (Thiéblemont et al., 2018) (Figure 1(C)). This morphological differentiation also reflects a geological division between an internal domain (Mayombe) and an external domain represent by the basin Niari-Nyanga Basin.

Form lithostratigraphy point of view, the West Congo belt consists of deformed and metamorphosed igneous and sedimentary rocks (Hossie, 1980; Boudzoumou & Trompette, 1988; Maurin et al., 1991; Affaton et al., 2016; Fullgraf et al., 2015) (Figure 2), which can be subdivided into two types of formations: 1) Paleoproterozoic formations represented by the Loeme Supergroup (Fullgraf et al., 2015; Affaton et al., 2016), corresponding to the western internal domain of the belt.

They consist of metasedimentary and reactivated granitoids during the Pan-African orogen; 2) Neoproterozoic formations composed of rift and post-rift deposits (Fullgraf et al., 2015) forming the external, eastern domain of the belt.

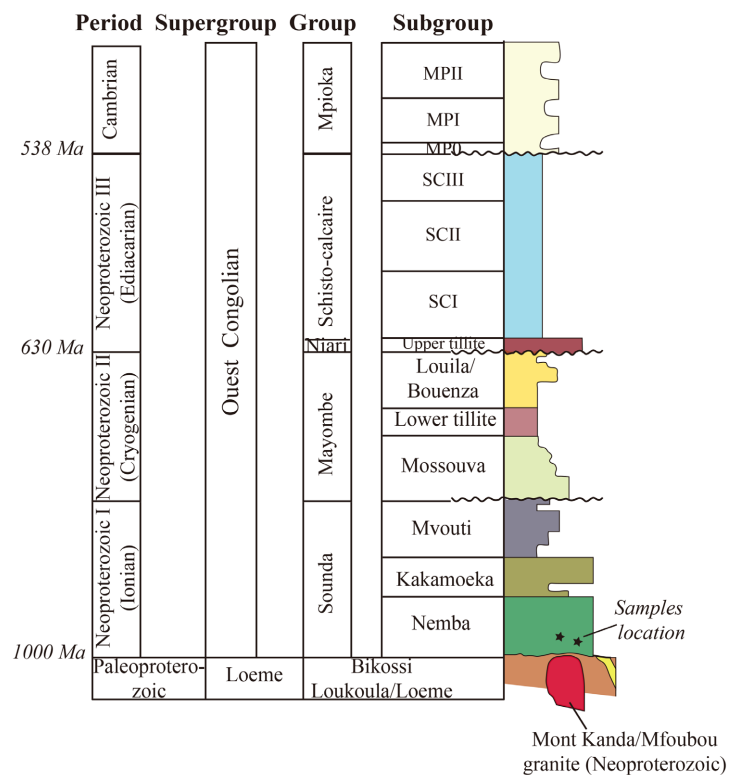


Figure 2. Simplified lithostratigraphy of the West Congo Supergroup in the Mayombe Belt according to Fullgraf et al. (2015), modified by Bazika et al. (2022).

The Paleoproterozoic formations are characterized by a gneissic substrate overlaid by volcanic and volcano-sedimentary deposits, as well as sediments related to Neoproterozoic tectonic extension. They consist of schists, ortho- and para-gneisses intersected by the Bilinga and Bilala metagranites, of U-Pb zircon ages of 2048 ± 12 Ma and 2014 ± 56 Ma, respectively (Affaton et al., 2016; Djama et al., 1992).

In the Brazilian segment of the Araçuaí-West Congo orogen, this domain is represented by the Paleo-mesoproterozoic Esinohaço Supergroup. This Supergroup comprises volcanics, quartz sandstones, conglomerates, pelites and subordinate carbonates (Dussin & Dussin, 1995; Uhlein et al., 1998; Martins-Neto, 2000).

The Neoproterozoic formations are defined by a metamagmatites and meta-sediments substrate and sedimentary rocks. They consist of the Sounda Group, corresponding to the intermediate domain, represented by the lower part of the West Congolian Supergroup (Tack et al., 2001; Fullgraf et al., 2015), including the Nemba Complex and the Kakamoeka and Mvouti Subgroups. The Nemba Complex is composed of metagabbros, metabasalts, amphibolites, and green schists. It is dated 915 ± 8 Ma, U-Pb zircon (Fullgraf et al., 2015). In the DRC, its equivalent (the basic rocks of Gangila from the Zadinien Group) has been dated between 999 ± 7 Ma and 920 ± 8 Ma (Tack et al., 2001).

The Kakamoeka Subgroup, or Mayumbian Group in the DRC, consists of volcano-sedimentary deposits, conglomerates, quartzites, graphitic schists, tuffs, pyroclastics, and mafic volcanics rocks. It has roughly the same age with the Nemba Complex (930 Ma to 910 Ma) (Tack et al., 2001; Fullgraf et al., 2015). The Mvouti Subgroup reflects the development of clayey sedimentation of turbiditic nature, originally rich in organic matter (Fullgraf et al., 2015), deposited in an aulacogenic basin (Boudzoumou & Trompette 1988); The Mayombe Group, including the Moussouva Subgroup in the intermediate domain, and the Lower Diamictite and Louila Subgroups in the external domain, representing the upper part of the Western Upper Congolian Supergroup. The Moussouva Subgroup is composed of quartzites and schists. The Lower Diamictite is composed of black clayey schists, shale, or massive rocks containing heterogeneous pebbles and cobbles (quartzite sandstones, quartz, subangular black jaspers, granites, coarse pyrite fragments), often stretched and parallel to the schistosity (Boudzoumou & Trompette, 1988; Affaton et al., 2016; Fullgraf et al., 2015; Delpomdor et al., 2019). Locally, this conglomerate contains metric lenses of quartzites (Boudzoumou, 1986). It is considered a glaciogenic conglomerate formed after a temporary emersion phase (Dadet, 1969; Boudzoumou & Trompette, 1988; Alvarez & Maurin, 1991). The Louila Subgroup is composed of silty and quartzose schists, arkosic meta-sandstones, occasionally oolitic limestones and marls (Boudzoumou & Trompette, 1988; Affaton et al., 2016; Fullgraf et al., 2015; Delpomdor et al., 2019). This subgroup is overlain by glaciomarine sediments (Upper Diamictite) (Boudzoumou & Trompette, 1988) of Marinoan age (Mickala et al., 2014), followed by the Schisto-Calcaire Group consisting of thick car-

bonate platform deposits (Dadet, 1969; Delpomdor et al., 2019; Mfere et al., 2020). The Schisto-Calcaire contains intercalations of shales and siltstones.

In the Araçuaí belt, the Neoproterozoic formations are represented by the Macaubas Group dated at approximately 1000 Ma and 850 Ma (Pedrosa-Soares et al., 2000; Uhlein et al., 1998). The Macaubas Group consists of tillite, sandstone, pelites, and subordinate basic volcanics rocks, distal pelites with intercalations of sandy turbidites (Uhlein et al., 1998; Martins-Neto et al., 2001) and an ophiolitic assemblage. The sedimentary rocks are considered deposits into a rift evolving into an oceanic basin (Pedrosa-Soares et al., 2000).

Structurally, the Mayombe Belt is a typically folded and thrust-belt towards the external domain. The internal domain is affected mainly by the Pan-African D2 deformation (Hossie, 1980; Boudzoumou & Trompette, 1988; Affaton et al., 2016; Le Bayon et al., 2015; Bouénitéla, 2019), marked by a strong NW-SE-trending S2 crenulation schistosity filling the Eburnean foliation (Boudzoumou & Trompette, 1988; Bouénitéla, 2019). Foliation is represented by the S1 flow schistosity. Locally, the S2 crenulation schistosity is overprinted by a third D3 deformation characterized by the S3 schistosity in the Loeme Group (Boudzoumou, 1986).

The intermediate and external domains of the Mayombe Belt are affected by two main Pan-African deformation stages primarily oriented NW-SE (Hossie, 1980; Maurin et al., 1991; Boudzoumou & Trompette, 1988; Affaton et al., 2016; Le Bayon et al., 2015; Bouénitéla, 2019). The first deformation stage (D1) is characterized by the S1 schistosity with eastward vergence and cross-cutting cleavage, affecting isoclinal folds in the intermediate domain and upright folds in the external domain. The second deformation stage (D2) is characterized by the S2 crenulation schistosity carried by upright folds in the intermediate domain. The S2 schistosity appears discretely in the external domain.

The grade of metamorphism decreases from the internal domain to the external. In the internal domain, metamorphism is characterized by the amphibolite facies, greenschist facies in the intermediate domain, and by the anchizonal facies in the external domain.

3. Methodology

The methodology used includes: 1) fieldwork based on the systematic description and sampling of various volcanic facies outcropping along the Moumba River (Figure 1(C)). Twenty-five (25) samples were collected and seventeen (17) representative samples of fresh rock were selected for laboratory analysis and studies. The geographic coordinates of all sampling points were determined using the global positioning system; 2) petrographic study has been done on thin section made at the University of Rennes 2, France. Microscopic petrographic descriptions were carried out at the Geodynamics Laboratory of Geosciences of Marien Ngouabi University.

Geochemical analyses of major, trace, and rare earth elements were performed

at the Laboratory of Petrographic and Geochemical Research (CRPG) of Nancy, France.

The samples were powdered, fused with LiBO_2 , diluted with HNO_3 , and analyzed by Inductively Coupled Plasma Mass Spectrometry (ICP-MS) and Inductively Coupled Plasma Optical Emission Spectrometry (ICP-OES). Quality control was carried out using international standards.

4. Results

4.1. Macroscopic Petrographic

The field descriptions show that the Moumba metasediments (**Figure 3(A)**, **Figure 3(B)**) consist mainly of quartz schists and green schists. The quartz schists and green schists are characterized by aggregates and/or lenses of quartz, exhibiting an S2 schistosity, trending $\text{N}150^\circ\text{-}30\text{SW}$; $\text{N}115^\circ\text{-}45\text{SW}$.

They are rich in both micas and rich in chlorite, giving them a micaschist appearance. The green schists alternate with quartz schists and form schistose layers, spanning several tens of meters. These metasediments belong to the Paleoproterozoic unit that constitutes the basement of the Mayombe belt.

The Moumba metabasites are green rocks rich in plagioclase and epidote, oriented along a crenulation schistosity (S2) dipping $\text{N}^\circ 140\text{-}50\text{ SW}$. They generally appear massive with a medium to fine grain. They include metagabbros, epidotites, amphibolites and chlorite schists (**Figure 3(D)**, **Figure 3(E)**, **Figure 3(C)** and **Figure 3(F)**).

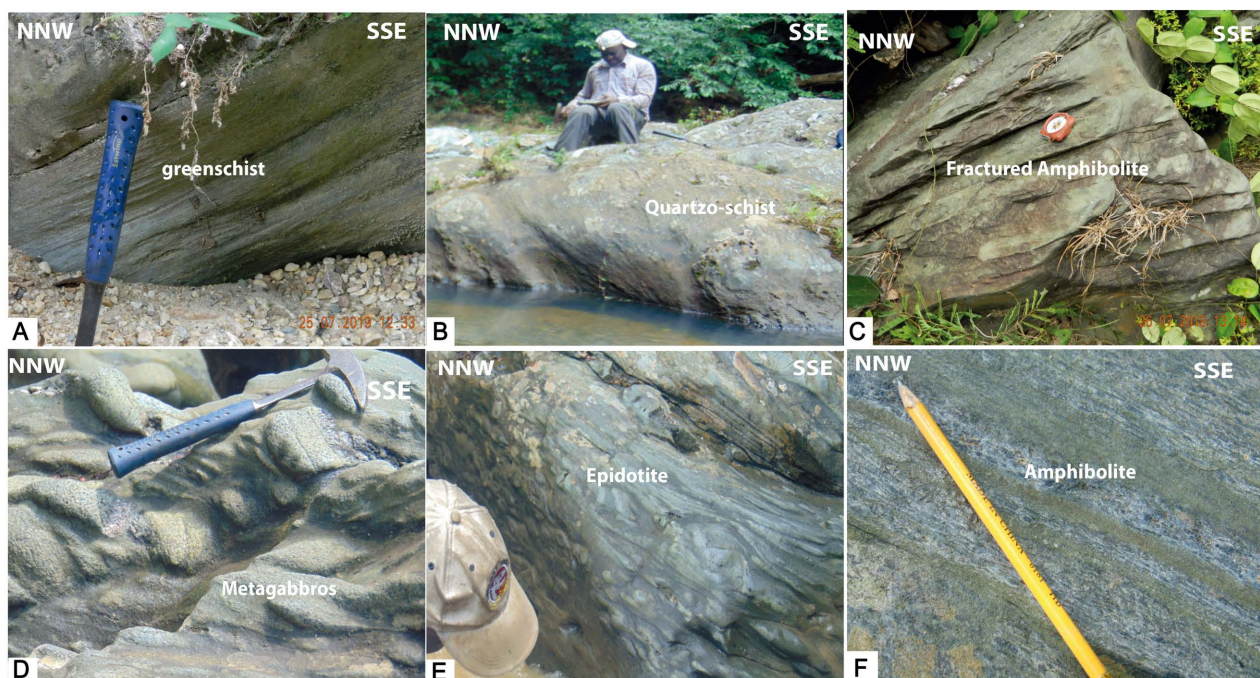


Figure 3. Outcrops of metasediments from the Bikossi unit and metabasites from Moumba. (A) Greenschist at the edge of the Moumba River; (B) Quartz schist containing quartz aggregates in the Moumba River; (C) Fractured amphibolites; (D) Metagabbros; (E) Epidotite containing nodules of gabbro; (F) Amphibolite with stretching lineation.

The amphibolites (**Figure 3(C)**, **Figure 3(F)**) are massive and locally exhibit a penetrative schistosity highlighted by biotite and amphibole. Locally, this plane carries a stretching mineral lineation (L1) dipping 40° towards the SSE, emphasized by hornblende porphyroblasts (**Figure 3(F)**). They are predominantly green, due to the abundance of amphibole and green to yellowish when they are rich in epidote.

The epidotites are greenish-yellowish epidote balls packed within the metagabbros. The metagabbros (**Figure 3(D)**) present, either massive appearance, with medium grain size or a foliated appearance with fine grain size.

4.2. Thin Section Description

The Thin section descriptions of the Mounba metabasites show that (**Figure 4(A)**, **Figure 4(B)**) the metagabbros show a porphyroblastic texture including hornblende phenocrysts and phantom pyroxene, oriented within a matrix of plagioclase, epidote, actinolite, quartz, calcite, sphene, and iron oxides (**Figure 4(A)**, **Figure 4(B)**). The primary metamorphic assemblage is characterized by Hbl + Pl + Bt, while the secondary assemblage consists of Pl (alb) + Ep + Chl ± Sp ± Op-Cal.

The amphibolites display a porphyroblastic texture (**Figure 4(C)**, **Figure 4(D)**). They are composed of hornblende, chlorite flakes, epidote grains, quartz-plagioclase associated with plagioclases, and some relics of biotite. All these minerals are oriented. The texture is characterized by a primary assemblage of Hb + Pl + Bt and a secondary assemblage of Pl (alb) + Chl + Act + Ep ± Op. Hornblende locally appears as stretched phenocrysts along the elongation direction, giving rise to pressure shadow structures (**Figure 4(C)**, **Figure 4(D)**).

The epidotites are characterized by a porphyroblastic texture. The foliation is rudimentary and defined by the orientation of actinolite needles and chlorite flakes (**Figure 4(E)**, **Figure 4(F)**).

They are primarily composed of epidote, constituting the matrix in which porphyroblasts of amphibole are embedded. Epidote occurs as fine isolated grains or clusters. Actinolite appears in acicular needle-like forms associated with chlorite. Hornblende persists as epidotized relic crystals, partially replaced by the secondary phase marked by actinote. The plagioclases form the matrix on which the other minerals tapise and constitute together with hornblende the primary metamorphic assemblage of Pl + Hbl + Bt. These epidotites contain numerous veins of minerals such as chlorite, epidote, quartz, and calcite, of hydrothermal origin, characterizing thus the secondary minerals assemblage of Ep + Act + Chl ± Cal ± Op.

The chlorite schists show a lepidogranoblastic texture and contain chlorite, quartz, epidote, and iron oxide (**Figure 4(G)**, **Figure 4(H)**). The schistosity is emphasized by the orientation of chlorite flakes. The overall crystal association defines a paragenesis of Pl + Chl + Ep + Qz ± Op.

4.3. Geochemistry

The results of geochemical analysis are reported in **Table 1(A)**, **Table 1(B)**.

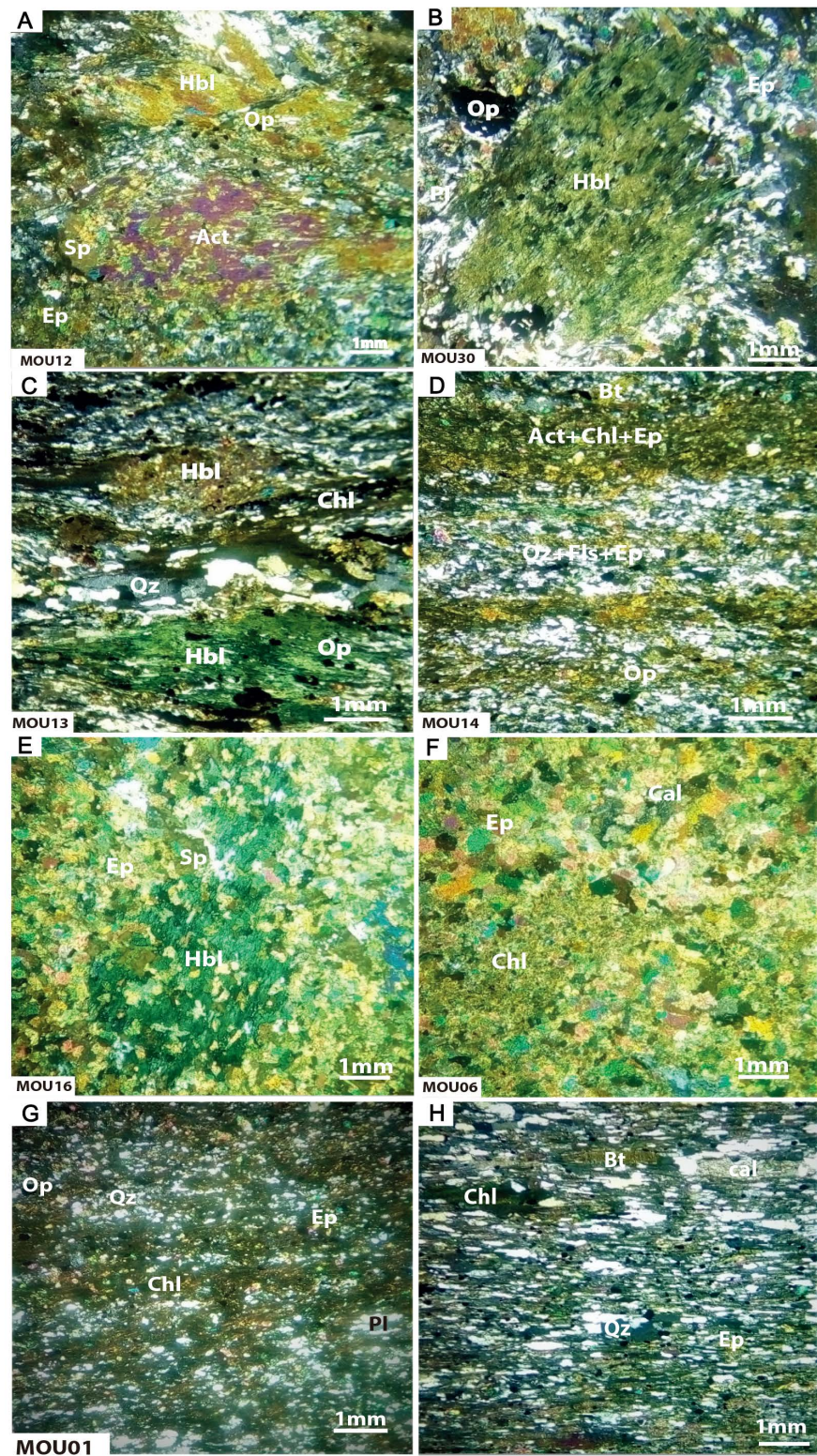


Figure 4. Microscopic images of Moubamba metabasites. Metagabbros [(A) Mou12, (B) Mou30]; Amphibolites [(C) Mou13, (D) Mou14]; Epidotite [(E) Mou16, (F) Mou06]; Green schists [(G) Mou01, (H) Mou01a]; Minerals: Act-actinolite, Pl-plagioclase, Ep-epidote, Chl-chlorite, Bt-biotite, Qz-quartz, Hbl-hornblende, Sp-spinel, Ap-apatite, Px-pyroxene, Op-opaque.

Table 1. (A): Analysis results of major and trace elements for samples of greenschist (01), epidotite (07). (B): Analysis's results of major elements and trace elements of amphibolite (04) and metagabbros (05) samples.

(A)								
Metabasites of Moumba								
Sample	Mou 01	Mou 05	Mou 16	Mou 7b	Mou 11	Mou 15	Mou 17	Mou 23
Petrology	Grenschtist				Epidotites			
SiO ₂	45.47	52.79	45.53	43.97	49.85	41.57	48.44	48.65
Al ₂ O ₃	16.10	13.77	13.60	16.08	11.61	15.88	14.01	9.86
Fe ₂ O ₃	14.43	12.76	13.82	14.87	14.16	14.46	12.63	15.07
MnO	0.18	0.28	0.19	0.20	0.30	0.26	0.18	0.23
MgO	5.70	5.87	4.35	6.32	6.54	5.42	4.53	8.11
CaO	5.55	4.87	16.27	7.82	11.40	13.45	13.03	10.99
Na ₂ O	4.42	4.25	1.53	3.90	3.01	2.16	2.90	2.66
K ₂ O	0.05	0.07	0.09	0.20	0.22	0.11	0.10	0.18
TiO ₂	3.41	1.68	1.65	2.23	1.17	1.39	1.35	2.36
P ₂ O ₅	0.37	0.39	0.40	0.49	0.34	0.41	0.37	0.14
PF	3.78	2.91	1.49	2.98	1.24	3.67	1.49	1.38
Total	99.44	99.65	98.92	99.06	99.83	98.78	99.04	99.62
As	1.44	1.36	1.74	1.54	1.92	1.87	2.66	1.42
Ba	196	122	34.8	164	137	99.0	105	113
Be	0.49	0.46	0.75	0.43	1.12	0.56	0.74	1.31
Bi	0.17	0.5	0.10	0.11	0.12	0.08	0.08	0.5
Cd	0.13	0.24	0.20	0.13	0.17	0.14	0.19	0.13
Co	50.4	51.9	29.7	60.2	50.3	46.6	41.4	53.2
Cr	90.0	66.7	81.5	90.5	52.0	83.7	72.3	68.1
Cs	0.02	0.05	0.09	0.65	0.73	0.13	0.05	0.25
Cu	55.1	24.0	44.8	39.0	49.2	42.0	252	76.4
Ga	20.9	15.9	21.9	24.4	17.7	26.6	19.7	13.6
Ge	2.19	1.15	2.62	1.84	2.16	2.03	2.42	1.95
Hf	3.79	2.15	2.59	3.15	1.77	2.36	2.18	2.67
Mo	0.5	0.5	0.5	0.5	0.5	0.5	0.5	0.71
Nb	14.4	7.47	7.48	9.53	5.07	6.07	5.69	10.2
Ni	102	108	103	131	121	122	95.6	143
Pb	6.69	2.29	6.90	4.73	5.18	7.08	5.02	3.75
Rb	0.39	0.73	0.79	7.19	4.96	1.18	0.69	4.08
Sb	0.37	0.21	0.22	0.33	0.34	0.35	0.28	0.27
Sc	55.47	28.20	35.34	38.38	23.54	28.66	30.93	31.78
Sr	301	157	532	349	364	486	593	184
Ta	1.01	0.55	0.52	0.66	0.36	0.44	0.39	0.68

Continued

Th	1.51	0.65	0.71	0.92	0.46	0.68	0.62	0.67
U	0.38	0.10	0.16	0.20	0.13	0.15	0.14	0.10
V	378	240	332	310	309	290	293	376
Y	40.0	19.6	20.3	27.6	15.1	21.3	19.2	17.6
Zr	151	84.7	109	123	72.4	102	92.6	113
La	21.1	10.7	12.4	15.7	8.50	12.8	10.4	9.07
Ce	46.4	21.8	26.5	31.6	18.0	26.8	22.4	19.3
Pr	6.09	2.80	3.52	4.21	2.24	3.46	2.96	2.52
Nd	26.7	12.2	15.7	18.3	10.0	15.4	13.4	11.0
Sm	6.56	3.01	3.75	4.48	2.34	3.73	3.17	2.55
Eu	2.56	1.11	1.33	1.92	0.983	1.49	1.23	0.921
Gd	6.78	3.03	3.71	4.54	2.41	3.79	3.31	2.62
Tb	1.13	0.515	0.604	0.747	0.410	0.607	0.534	0.439
Dy	7.40	3.39	3.73	4.85	2.71	3.83	3.40	3.02
La/Ta	21.02	19.64	23.96	23.94	23.74	29.37	26.58	13.41
La/Th	14.03	16.61	17.60	17.03	18.30	18.80	16.85	13.62
Th/Ta	1.50	1.18	1.36	1.41	1.30	1.56	1.58	0.98
Th/La	0.07	0.06	0.06	0.06	0.05	0.05	0.06	0.07
Sm/Y	0.16	0.15	0.19	0.16	0.15	0.18	0.16	0.15

(B)

Metabasites of Moumba

Sample	Mou13	Mou19	Mou20b	Mou21	Mou25	Mou28	Mou31	Mou12	Mou30
Petrology	Amphibolites			Metagabbros					
SiO ₂	46.35	44.78	46.93	42.02	43.95	46.49	45.20	42.64	41.56
Al ₂ O ₃	15.87	15.25	14.64	14.68	15.46	14.63	17.42	16.24	15.94
Fe ₂ O ₃	13.69	14.96	14.19	16.37	14.77	13.63	13.09	15.67	14.90
MnO	0.18	0.21	0.19	0.22	0.23	0.21	0.25	0.24	0.24
MgO	5.77	7.67	7.05	8.51	6.93	6.56	6.02	7.70	6.87
CaO	8.13	7.93	7.32	7.89	8.37	8.83	10.87	8.43	9.12
Na ₂ O	4.06	3.57	4.21	2.78	3.20	3.65	2.64	3.07	3.45
K ₂ O	0.11	0.15	0.12	0.10	0.13	0.13	0.13	0.10	0.19
TiO ₂	1.87	1.73	1.73	2.39	1.84	1.38	1.03	1.65	1.83
P ₂ O ₅	0.56	0.55	0.46	0.62	0.56	0.62	0.19	0.67	0.78
PF	2.80	2.86	2.60	3.63	3.50	2.76	3.23	3.69	5.03
Total	99.38	99.66	99.45	99.19	98.95	98.87	100.05	100.09	99.89
As	1.54	1.10	1.25	4.81	1.54	1.46	1.28	1.74	2.70
Ba	78.0	61.3	54.7	26.1	86.1	68.2	69.6	51.6	238
Be	0.46	0.53	0.67	0.74	0.54	0.62	0.50	0.48	0.37

Continued

Bi	0.10	0.09	0.12	0.11	0.16	0.05	0.05	0.06	0.11
Cd	0.11	0.11	0.08	0.24	0.13	0.10	0.16	0.12	0.18
Co	51.5	61.6	57.8	65.2	63.7	54.0	40.4	66.4	67.9
Cr	79.8	82.2	81.7	90.0	94.7	84.7	56.5	85.0	86.9
Cs	0.16	0.20	0.10	0.11	0.17	0.13	0.07	0.14	0.36
Cu	145	18.0	72.1	89.2	9.5	28.2	4.1	96.6	438
Ga	23.5	18.9	18.2	20.6	21.4	18.5	28.9	24.4	25.1
Ge	1.59	1.67	1.35	1.56	1.70	1.79	3.12	1.73	1.70
Hf	2.74	2.99	2.44	3.40	2.70	3.46	2.38	3.24	2.97
In	0.07	0.09	0.06	0.06	0.07	0.07	0.08	0.09	0.08
Mo	0.54	0.5	0.5	0.60	0.5	0.5	0.5	0.82	0.95
Nb	7.74	7.15	7.10	10.1	7.52	5.75	6.45	7.13	7.94
Ni	114	119	121	146	130	107	83.7	135	136
Pb	4.54	6.69	2.29	6.90	4.73	5.18	7.08	5.02	3.75
Rb	1.09	1.72	0.94	1.71	2.40	1.47	2.52	2.24	3.74
Sb	0.35	0.26	0.20	0.22	0.49	0.25	2.24	0.28	0.35
Sc	33.84	39.00	31.24	32.83	34.38	32.08	24.40	36.54	32.90
Sn	0.69	0.71	0.69	0.70	0.70	0.56	0.58	0.70	0.79
Sr	332	207	178	231	249	256	1039	344	277
Ta	0.54	0.50	0.50	0.70	0.55	0.41	0.40	0.52	0.56
Th	0.74	0.98	0.66	0.74	0.79	0.85	0.78	1.03	0.89
U	0.17	0.20	0.13	0.14	0.10	0.15	0.19	0.21	0.18
V	296	292	282	300	299	277	229	302	297
Y	23.5	26.0	20.0	23.5	21.6	23.3	21.6	28.0	27.4
Zn	110	140	126	163	141	123	174	146	142
Zr	115	125	99.9	143	112	111	89.9	137	125
La	12.7	14.7	10.2	11.1	13.3	13.4	13.6	16.0	15.4
Ce	26.5	31.9	21.9	23.9	28.7	29.6	26.0	34.6	33.3
Pr	3.44	4.26	2.90	3.18	3.65	3.94	3.15	4.56	4.43
Nd	15.3	19.0	13.0	14.3	16.0	17.8	13.4	20.5	20.0
Sm	3.72	4.55	3.09	3.50	3.83	4.35	3.41	4.86	4.71
Eu	1.61	1.71	1.27	1.27	1.52	1.36	1.37	1.83	1.94
Gd	3.87	4.72	3.29	3.64	3.91	4.42	3.64	4.94	4.82
Tb	0.645	0.776	0.546	0.620	0.631	0.697	0.615	0.824	0.793
Dy	4.23	4.89	3.51	4.16	3.99	4.44	3.94	5.08	5.05
La/Ta	29.24	20.48	15.90	24.41	32.82	33.95	31.04	27.29	29.24
La/Th	15.09	15.42	15.01	16.84	15.80	17.54	15.56	17.37	15.09
Th/Ta	15.09	15.42	15.01	16.84	15.80	17.54	15.56	17.37	15.09
Th/La	1.94	1.33	1.06	1.45	2.08	1.94	1.99	1.57	1.94
Sm/Y	0.18	0.15	0.15	0.18	0.19	0.16	0.17	0.17	0.18

The metabasites from Moumba exhibit a varied chemical composition, with SiO_2 content ranging from 40.65% to 52.79%, Al_2O_3 ranging from 9.86% to 17.46%, Fe_2O_3 varying from 12.63% to 16.37%, MnO ranging from 0.18% to 0.30%, MgO ranging from 2.86% to 8.51%, CaO ranging from 4.87% to 18.74%, Na_2O varying between 1.09% and 4.42%, K_2O ranging from 0.05% to 0.22%, with low TiO_2 values < 2 , except for three samples (Mou3, Mou7b, and Mou23) showing $\text{TiO}_2 > 2$, and P_2O_5 ranging from 0.14% to 0.67%. The sum of $\text{Fe}_2\text{O}_3 + \text{MgO} + \text{MnO} + \text{TiO}_2$ varies from 18.37% to 27.54%, and $\text{Na}_2\text{O} + \text{K}_2\text{O}$ from 1.15% to 4.6%. The contents of certain transition elements such as Co, Cr, Ni, and V range respectively between 24.7 and 66.4 ppm, 52.0 and 90 ppm, 66.1 and 146 ppm, and 277 and 378 ppm.

The Harker diagram of major elements vs Zr (**Figure 5**) shows positive linear correlations for MgO , Fe_2O_3 , TiO_2 , and P_2O_5 , whereas SiO_2 shows a negative linear correlation. The concentrations of CaO , Na_2O , K_2O , and Al_2O_3 are relatively variable and exhibit a wide scatter of points.

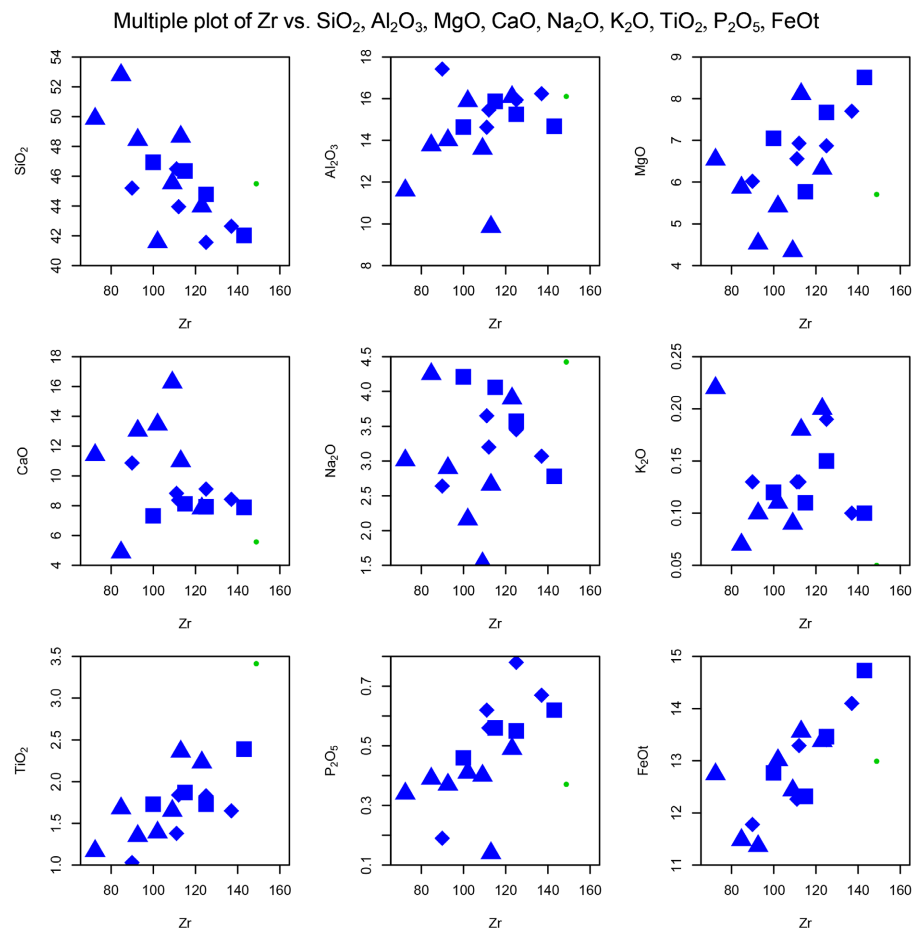


Figure 5. Harker diagrams showing random correlations between oxides (Al_2O_3 , CaO , K_2O , P_2O_5 , Na_2O) with Zr and linear correlations between oxides (SiO_2 , Fe_2O_3 , TiO_2 , MgO) with Zr in the metabasite rocks from Moumba. The x-axis represents the Zr content taken as an index of magmatic differentiation. The y-axis represents the concentrations of oxides and other trace elements. The oxide contents are expressed in weight percentage.

The LILE vs Zr display a wide scatter of points and do not display any linear correlation. In contrast, transition elements such as Cr and Ni, HFSE, and REE plotted against Zr, define relatively immobile trends with positive linear correlation with the differentiation index (Zr) (**Figure 6**).

The diagram by Winchester & Floyd (1977) modified by Pearce (1996) (**Figure 7(A)**), plots all the metabasites of Moumba in the field of subalkaline basalts. The diagram by Ross & Bédard (2009) (**Figure 7(B)**) groups all the samples in the field of transitional basalts and shows Th/Yb and La/Yb ratios ranging respectively from 0.2 to 0.4 and from 4.40 to 6.6.

These metabasites have rare earth element (Σ REE) contents ranging from 51.63 to 135.58 ppm. In the chondrite-normalized diagram by Nakamura (1977) (**Figure 8**), the studied samples show nearly identical and parallel patterns with a negative slope inside LREE, and flat patterns inside HREE.

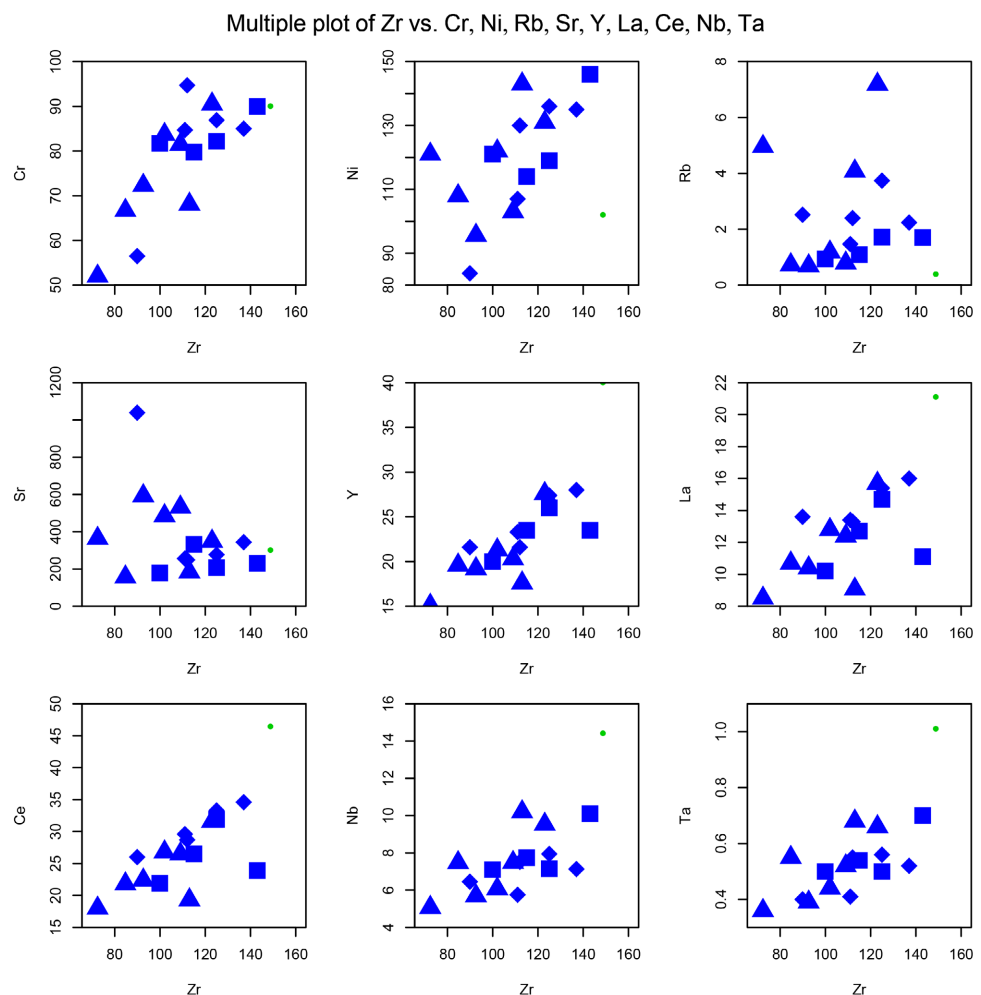


Figure 6. Harker diagrams showing random correlations between Rb, Sr and Ni with Zr and linear correlations between transition elements Cr, La, Ce, Y, Nb and Ta with Zr in the metabasites of Moumba. The x-axis corresponds to the Zr content taken as an index of magmatic differentiation. The y-axis corresponds to the concentrations of oxides and other trace elements. Trace elements are expressed in ppm.

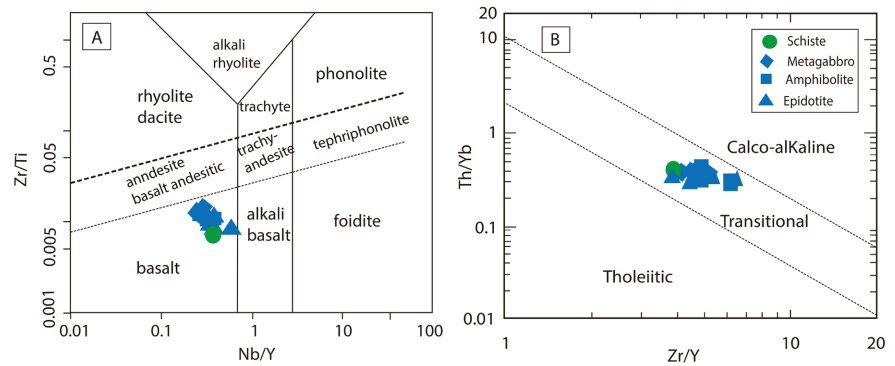


Figure 7. Classification of metabasite rocks from Moumba in the Nb/Y-Zr/Ti and Th/Yb vs Zr/Ti diagrams by Pearce (1996: Figure 7A) and Ross & Bédard (2009: Figure 7B). The samples fall within the field of basalts and transitional basalts.

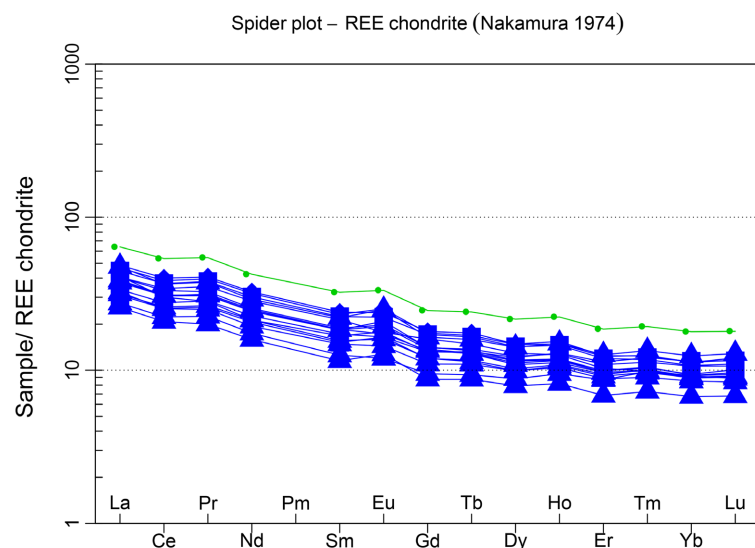


Figure 8. Chondrite normalized rare earth elements (REE) patterns of the Moumba metabasites. Values used are those of Nakamura (1977). The metabasites exhibit a negative trend enriched in LREE/HREE with positive Eu anomalies.

They are significantly enriched in LREE compared to HREE. The different fractionation ratios are high: (La/Yb) $N = 2.97 - 4.49$ and (La/Sm) $N = 1.94 - 2.28$. The REE patterns show positive Eu anomalies, except the sample MO28 which exhibits a negative Eu anomaly ($Eu^*/Eu = 0.95$).

The Moumba patterns normalized to the primitive mantle of McDonough & Sun (1995) (Figure 9) are characterized by the absence of negative anomalies in Nb-Ta and Ti. They are enriched in LILE and show a low fractionation rate in HFSE, strong positive anomalies in Ba, Sr, Pb, and negative anomalies in Rb.

The projection onto the Zr vs Zr/Y diagram by Pearce & Norry (1979) (Figure 10(B)) and Yb vs. Th/Ta diagram by Schandl & Gorton (2002) (Figure 10(C)) plots the majority of samples in the within-plate basalts field, except two samples located outside the distinguished fields.

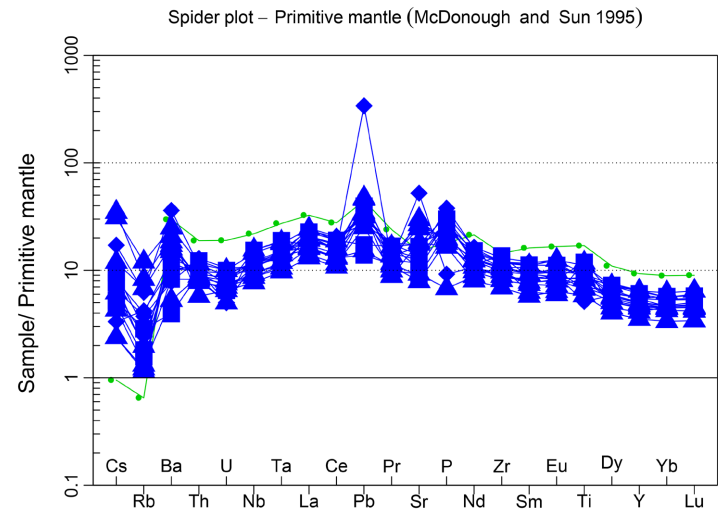


Figure 9. Trace-element diagram of Moumba metabasites normalized to the primitive mantle of McDonough & Sun (1995). All metabasites exhibit positive Pb anomalies.

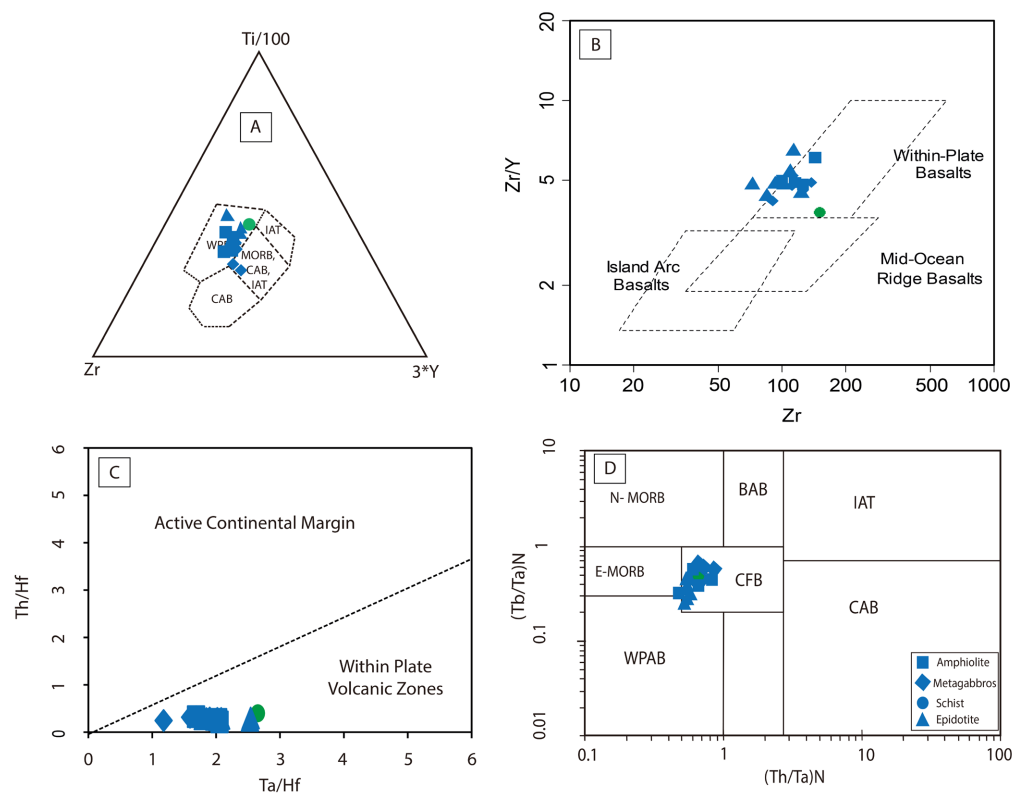


Figure 10. Discrimination diagrams for trace elements of the Moumba metabasites. (A) $Zr/4$, $Ti/100$, and $Y*3$ triangular diagram Pearce and Cann (1973), the metabasite samples tend towards within-plate continental alkali basalts, but two metagabbros show tholeiitic affinity of island arcs. (B) Zr vs. Zr/Y Pearce & Norry (1979). (C) Ta/Hf vs. Th/Hf Schandl & Gorton (2002). (D) $(Tb/Ta)N$ vs. $(Th/Ta)N$ Thiéblemont et al. (1994). The metabasites plots in the within-plate domain. Abbreviations: E-MORB: enriched mid-ocean ridge basalt, N-MORB: normal to mid-ocean ridge basalt, CAB: volcanic arc basalt, WPB: within-plate basalt; WPAB: within-plate alkali basalt, BAB: back-arc basin basalts; IAT: island arc tholeiite, CFB: continental flood basalt.

In the Th/Ta and Tb/Ta diagram by [Thiéblemont et al. \(1994\)](#) (**Figure 10(D)**), the metabasites fall in the CFB field, whereas in the Zr/4-2Nb-Y diagram by [Pearce and Cann \(1973\)](#) (**Figure 10(A)**), they are distributed in the within-plate lavas field, except two samples Mou23 and Mou01, which fall into the field of island arc tholeiites, MORB, and continental alkali basalts.

5. Discussion

5.1. Petrochemical Characteristic

The results of the petrographic study reveal that the study area is characterized by a well-preserved upper crustal volcano-felsic assemblage represented by interstratified metabasites in metasediments. The coexistence of Hb + Ep + Pl + Bt in the metabasites indicates that the rocks of Moumba underwent lower amphibolite grade of metamorphism. The secondary paragenesis Pl (Alb) + Act + Chl + Ep ± Cal ± Op reflects a retromorphose towards greenschist grade. The Moumba metabasites are affiliated with the Nemba Complex dated between 915 Ma and 1000 Ma ([Le Bayon et al., 2015](#); [Fullgraf et al., 2015](#)). The heterogeneity of textures and rocks nature suggest a gabbroic or doleritic protolith.

The geochemical characteristics show that Moumba metabasites are mainly composed of transitional subalkaline basalts poor in TiO₂ (Low-Ti) and MgO with a strong enrichment in Fe₂O₃ (t) (13.95% - 16.37%). The fairly significant variations in alkali contents Na₂O (1.09% - 4.42%) and the high values of Al₂O₃ suggest extensive feldspar albitization ([Talbi et al., 2005](#)).

5.2. Tectonic Discrimination

The content of immobile HFSE elements used to constrain the tectonic setting of volcanic protoliths, discriminates the Moumba metabasites in an intraplate context. High Y and Zr contents, along with high Zr/Y ratios > 1.5, characterize, according to [Pearce & Norry \(1979\)](#); [Pearce \(1983\)](#), an intraplate continental basalt environment of the CFB type (**Figure 10**). Similarly, the values of the La/Sm and Gd/Yb ratios of REE normalized to N-MORB vary from 2 to 23 and from 0.5 to 3.5, respectively. They are similar to those reported for Deccan-type basalts by [Lightfoot et al. \(1990\)](#); [Mahoney et al. \(2000\)](#). Furthermore, the absence of negative anomalies of Nb, Ta, and Ti (**Figure 9**), characteristic of a subduction or arc environment, excludes the emplacement of Moumba metabasites in the context of an active margin related to a subduction zone forming volcanic arcs. Instead, it suggests emplacement in a passive margin setting.

The diagram of [Pearce & Cann \(1973\)](#) (**Figure 10(A)**) suggests a continental arc character with enrichment in MORB. The arc signature of these rocks may suggest crustal involvement and a decrease in mantle melting degrees ([Wilson, 1989](#)). These characteristics are in line with the interpretation suggested by [Bazika et al. \(2022\)](#) for the equivalents basic rocks of Loukounga in the southern part of Mbena and by for the Gangila basalts of the Zadinian Group in the D.R. Congo and dated between 930 Ma and 920 Ma [Tack et al. \(2001\)](#). Our results al-

so conform to the Tack et al. (2001) model proposed by Cavalcante et al. (2019) for basalts of the Macaúbas group in the Brazilian margin in the Araçuaí belt. Cavalcante et al. (2019) question the possible existence of oceanic crust. According to Cavalcante et al. (2019), the model involving about 50 Ma of subduction of oceanic crust and the development of the related arc cannot be compatible with the emplacement of Neoproterozoic magmatic rocks in the Araçuaí-West Congo Belt. They propose an intracontinental hot orogeny model, where significant melting of the middle crust could have caused the propagation of the upper crust in an orogenic setting created by collisions along the N, W, and S margins of the São Francisco craton from 630 Ma onward.

In conclusion, this magmatism reflects heterogeneity in the composition of the lithospheric source and probably different rates of partial mantle melting. Despite the calc-alkaline nature (Boudzoumou, 1986; Djama et al., 1988; Fullgraf et al., 2015; Djama et al., 2018) of the acid-basic rocks emplaced during this period, it does not seem that a genetic link with oceanic crust subduction can be invoked. The Neoproterozoic paleogeography (Rodinia) is marked by intracontinental rifts (Kampunzu & Cailteux, 1999; Trompette, 2000), indicating an intraplate continental environment. The calc-alkaline signature may be due to partial melting in an extensional setting of a metasomatized mantle (McCulloch & Gamble, 1991) during an ancient, presumably Eburnean subduction (Piqué et al., 1998). Thus, the volcanism of the metabasites of Moumba was effectively established in a context of continental flood basalts (CFB).

5.3. Petrogenesis

5.3.1. Fractional Crystallization

The trends of major and trace elements in the Harker diagrams (Figure 5, Figure 6) indicate that positive linear correlations may be related to the fractionation of olivine, pyroxene, and plagioclase. This fractionation is consistent with fractional crystallization and forms, for the Moumba metabasites, a continuous co-genetic evolutionary trend similar to those observed in continental basalts (Bellieni et al., 1984; Piccirillo et al., 1988; Marques et al., 1999; Rocha-Júnior et al., 2013). However, some scattering of points indicates a random evolution. This suggests that, simple binary mixing mechanisms must have played a role in the origin of differentiation lineages. The positive anomalies in Eu (Figure 8) in the majority of samples suggest an accumulation of plagioclase in the magma and the presence of garnet in the residue.

5.3.2. Crustal Contamination

Some chemical characteristics of volcanic rocks can be acquired through interactions with crustal rocks during the transfer of magma from the mantle to the surface and also during the storage of these magmas in crustal magma chambers at different levels and their differentiation through crystalline fractionation (Kamgang et al., 2008). These interactions have already been observed and characterized by Bazika et al. (2022) in the Loukounga metabasites.

In the Zr/Ti/100-3*Y diagram (Pearce & Cann, 1973) (Figure 10), the random correlations of concentrations of certain major elements (CaO, Na₂O, K₂O, and Al₂O₃) and trace elements (Rb, Sr) seem to indicate possible crustal contamination of the magma. The absence of Nb-Ta anomalies in the chemical composition of the igneous rocks may suggest that they have not been affected by crustal contamination and/or its effect is negligible (Nagudi & Coll, 2003; Fatehi & Ahmadi-pour, 2018). However, Frey et al. (2002), Wooden et al. (1993), Xia & Li (2019) suggest that high ratios of (Th/Ta) > 1.5, (La/Ta) > 22, and low ratios of (Th/La) < 1, (Nb/La) < 1 would indicate crustal contamination of the magma. The majority of metabasites show high ratios of (Th/Ta) > 1.5, (La/Ta) > 22, and low Th/La, Nb/La ratios, respectively less than 1. Figure 11 shows positive correlations between Zr vs. Nb and (Sm/La)N vs. (Gd/Yb)N, indicating clearly that the chemical variations observed in the metabasites of Moumba were mainly acquired through interaction with crustal rocks during the differentiation of the magma.

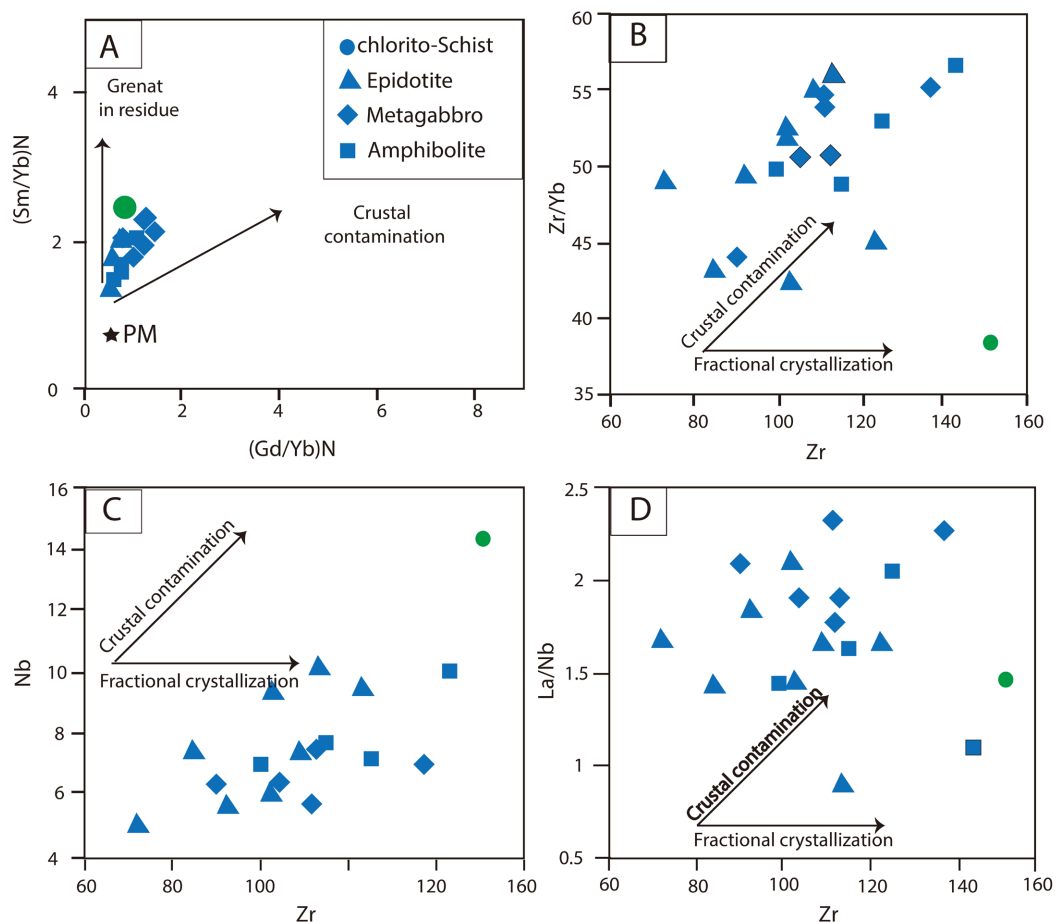


Figure 11. Crustal contamination discrimination diagrams. All diagrams indicate the contribution of crustal contamination to the metabasites; (A) (Sm/Yb) vs (Th/Nb) diagram from Wang et al. (2007) normalized to the primitive mantle of Sun & McDonough (1989); (B) Zr/Yb vs Zr diagrams of the Moumba metabasites. D) La/Nb vs Zr diagram of the metabasites. (C) Nb vs Zr diagram of the metabasites. The indicative trends of fractional crystallization and crustal contamination confirm that the basic magmas of Moumba interacted with continental crustal rocks.

The Zr/Yb and La/Nb ratios are also well correlated with Zr contents, compatible with contamination by a high La/Nb component, typical of continental crustal rocks (Figure 11).

This crustal component also has a very high Pb content. This process of contamination by a crustal component with a high Pb content has already been observed in other trap basalts (Mahoney et al., 2000; Beard et al., 2017). This indicates that the Moumba metabasites are contaminated by a crustal component.

5.3.3. Mantle Source Nature

The ratios of immobile trace elements such as Th and Yb are independent of mineral sources, the degree of partial melting, and fractional crystallization, meaning that their ratios reflect the mantle source (Aldanmaz et al., 2000; Roland et al., 2000). In the Nb/Yb vs. Th/Yb diagram (Pearce, 1983; Pearce, 2008) (Figure 12(A)) and Nb/Th vs. Zr/Nb (Condie, 2005) (Figure 12(D)), the metabasites fall into the field of mantle-derived fusion enriched parallel to the intraplate enrichment trend (W trend).

In the Zr/Y vs. Nb/Y diagram (Fitton et al., 1997) (Figure 12(B)), the Moumba metabasites trace in the enriched MORB field. This configuration suggests that

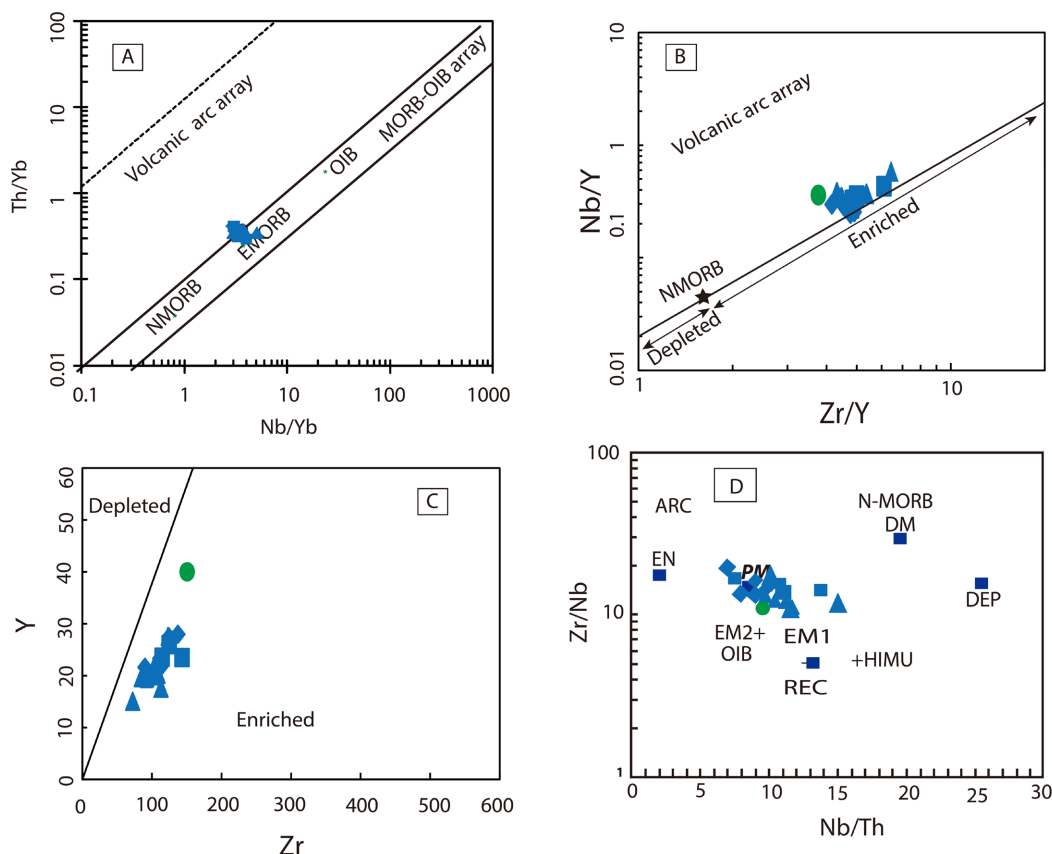


Figure 12. Discrimination diagrams for determining the possible source of Moumba metabasites. (A) Th/Yb vs. Nb/Yb (Pearce, 2008). (B) Zr/Y vs. Nb/Y (Fitton et al., 1997); (C) Zr vs. Y (Coban & Flower, 2007). The Moumba metabasites fall into the enriched mantle field.

these metabasites originate from an enriched mantle plume. The Ti/Y and Nb/Y ratios in intraplate basalts are higher than in other basalts. These differences indicate that the mantle source of these rocks is more enriched compared to MORB and volcanic arc basalt sources (Rollinson, 1996). High Ti/Y and Nb/Y ratios in the studied metabasites suggest an enriched mantle source of their primitive magmas. According to Sun & McDonough (1989), Zr/Y ratios > 2.46 and Zr/Nb ratios < 15.71 separate enriched sources from depleted sources in basalts. The Zr/Y ratio (3.76 to 6.44) and Zr/Nb ratio (10.46 to 19.32) in the metabasites indicate their derivation from an enriched mantle source. On the Zr vs. Y diagram (Coban & Flower, 2007) (Figure 12(C)), the metabasites fall into the enriched field. This configuration suggests that the metabasites of Mounba derive from an enriched mantle plume head.

5.3.4. Condition and Degree of Partial Melting

The gradient of REE spectra in any suite of igneous rocks helps to understand the depth and degree of melting conditions (Cullers & Graf, 1984; Fram & Lesher, 1993; Hirschmann et al., 1998; Patel et al., 2021). The REE abundances

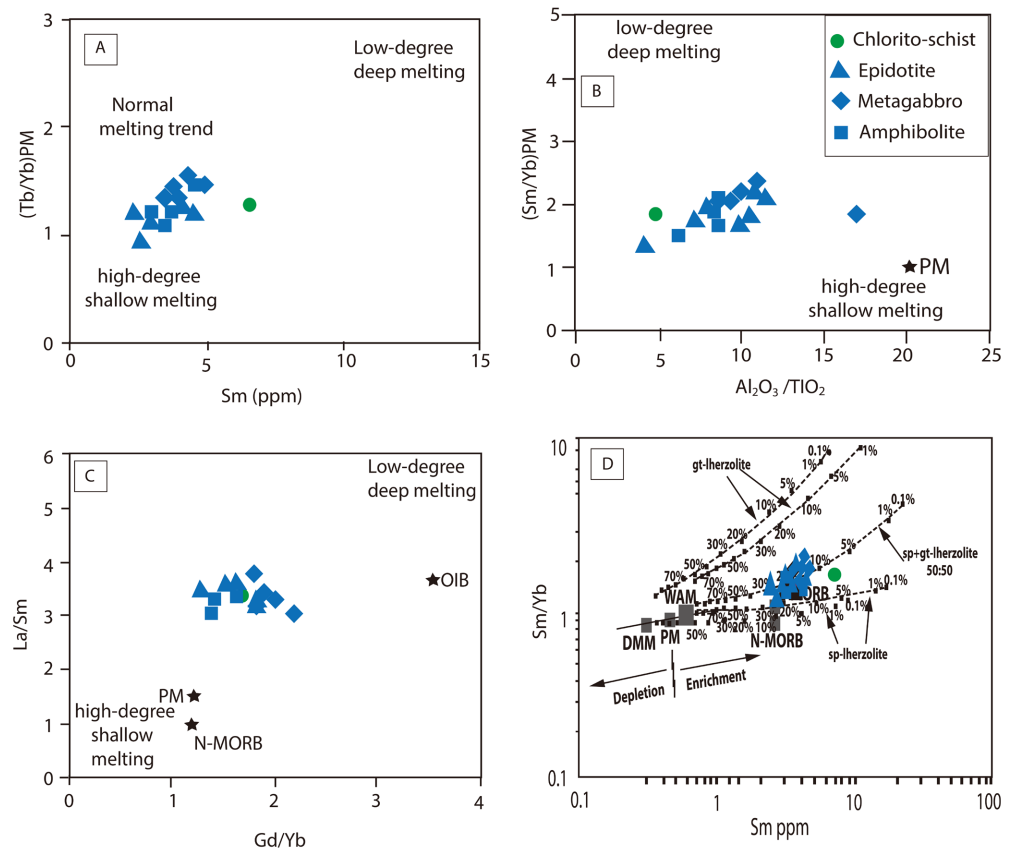


Figure 13. Discrimination diagram to determine the conditions and degree of magma partial melting. (A) Sm Vs (Tb/Yb)PM, (B) Al₂O₃/TiO₂ vs (Sm/Yb)PM, (C) Gd/Yb vs. La/Sm (Wang et al., 2007); the Mounba metabasites fall into deep low-degree melting and shallow high-degree melting; (D) Sm VS; Sm/Yb (Aldanmaz et al., 2000), all metabasites fall on the curve of partial melting ranging from 10% to 30%, containing 10% to 30% lherzolite with spinel and garnet.

normalized to chondrites define the presence or absence of residual garnet in the source region (Jung, 2000; Patel et al., 2021; Hirschmann et al., 1998; Green, 1994). The REE spectra of Moumba are enriched in LREE and inclined, showing a negative trend (Figure 8). They have relatively high (Gd/Yb)PM ratios (1.44 to 2) and (Tb/Yb)PM ratios (1.10 to 1.53). This indicates the presence of residual garnet during partial melting (Green, 1994). Since garnet retains HREE from the mantle during partial melting, YbN values < 10 (4.24 and 8.91) in the metabasites suggest, according to Wilson (1989); Oliveros et al. (2007), the presence of garnet as a residual phase in the source region. Diagrams Sm vs. (Tb/Yb)PM, Al_2O_3/TiO_2 vs (Sm/Yb)PM, and Gd/Yb vs. La/Sm by (Wang et al., 2007) (Figures 13 (A)-(C)) shows that the Moumba metabasites fall between the fields of deep mantle low-degree melting and shallow mantle high-degree melting fields.

However, the relatively moderate Al_2O_3/TiO_2 ratios (4.72 - 11.42) and high (Sm/Yb)PM ratios (1.37 - 2.33) indicate lower degrees of partial melting from a relatively shallower mantle source (Figure 13). In the Sm/Yb vs Sm diagram (Figure 13(D)), these metabasites plot on the lherzolite - spinel + garnet curve, confirming thus the presence of garnet in the source region, and hence, the magma likely resulted from a shallower partial melting of the mantle containing 50% spinel and 50% regolith. It is highly probable that the Moumba metabasites were generated from a significantly enriched mantle, which began melting in the garnet facies stability zone and continued melting in the spinel facies stability zone. The degree of partial melting, following the parameters of Aldanmaz et al. (2000) (Figure 13), was probably less than 30% (Figure 13(D)).

6. Conclusion

This study, which aims to constrain the geochemical signature of the Nemba complex of the West Congo belt, constitutes a contribution to the reconstruction of the geodynamic context of the metabasites of the Pan-African Araçuaí-West Congo belt. It shows that Moumba metabasites correspond to Nemba complex of West Congo Belt and are made up of amphibolites, metagabbros, epidotites and green schists interstratified in the Eburnean metasediments. The geochemical signature highlights continental flood basalts (CFB), emplaced in an intraplate geodynamic context from magma coming from an enriched mantle plume having undergone partial melting of low degrees. This magma was subsequently contaminated by continental lithospheric during their ascent. This present study calls into question the possible existence of oceanic crust and the presence of the ophiolite complex in the West Congo belt. We support the intracontinental model for the formation of the West Congo belt. Our results suggest that the West Congo belt was formed following the closure of a continental rift due to continental collision. This hypothesis is in agreement with recent data obtained throughout the Araguaí-West Congo Belt.

The understanding would only be better if we added isotope, microprobe and structural analyses to the protocol to better understand the geochemical signa-

ture, the P-T-t paths and the markers of Pan-African tectogenesis of the metabasites of the Nemba complex and the associated lithological units. These additional analyses will make it possible to precisely establish correlations on the scale of the West-Congolian Belt, and also on the scale of the Araçauí-West Congo orogen.

Conflict of Interest

The authors declare that no conflicts of interest relevant to this study.

References

- Affaton, P., Kalsbeek, F., Boudzoumou, F., Trompette, R., Thrane, K., & Frei, R. (2016). The Pan-African West Congo Belt in the Republic of Congo (Congo Brazzaville): Stratigraphy of the Mayombe and West Congo Supergroups Studied by Detrital Zircon Geochronology. *Precambrian Research*, 272, 185-202. <https://doi.org/10.1016/j.precamres.2015.10.020>
- Aldanmaz, E. R. C. A. N., Pearce, J. A., Thirlwall, M. F., & Mitchell, J. G. (2000). Petrogenetic Evolution of Late Cenozoic, Post-Collision Volcanism in Western Anatolia, Turkey. *Journal of Volcanology and Geothermal Research*, 102, 67-95. [https://doi.org/10.1016/S0377-0273\(00\)00182-7](https://doi.org/10.1016/S0377-0273(00)00182-7)
- Alkmim, F. F., Marshak, S., Pedrosa-Soares, A. C., Peres, G. G., Cruz, S. C. P., & Whittington, A. (2006). Kinematic Evolution of the Araçauí-West Congo Orogen in Brazil and Africa: Nutcracker Tectonics during the Neoproterozoic Assembly of Gondwana. *Precambrian Research*, 149, 43-64. <https://doi.org/10.1016/j.precamres.2006.06.007>
- Alvarez, P., & Maurin, J.-C. (1991). Sedimentary and Tectonic Evolution of the Upper Proterozoic Comba Basin (Congo): Sequence Stratigraphy of the West-Congolian Supergroup and Strike-Slip Damping Model in the Context of Pan-African Tectogenesis. *Precambrian Res*, 50, 137-171. [https://doi.org/10.1016/0301-9268\(91\)90051-B](https://doi.org/10.1016/0301-9268(91)90051-B)
- Bazika, U. V. M., Bouénitéla, V. T. T., Lekeba, N. M., & Boudzoumou, F. (2022). Petrology and Geochemistry of Loukounga Metabasites Rocks: Constraining the Geodynamic Context of Neoproterozoic Nemba Complex in the Mayombe Belt. *Open Journal of Geology*, 12, 919-946. <https://doi.org/10.4236/ojg.2022.1211044>
- Beard, C. D., Scoates, J. S., Weis, D., Bédard, J. H., & Dell'Oro, T. A. (2017). Geochemistry and Origin of Neoproterozoic Flood Basalts from Natkusiak and Related Franklin Sills, Victoria Island, Arctic Canada. *Journal of Petrology*, 58, 2191-2220. <https://doi.org/10.1093/petrology/egy004>
- Bellieni, G., Comin-Chiaramonti, P., Marques, L. S., Melfi, A. J., Piccirillo, E. M., Nardy, A. J. R., & Roisenberg, A. (1984). High- and Low-TiO₂ Flood Basalts from the Paraná Plateau (Brazil): Petrology and Geochemical Aspects Bearing on Their Mantle Origin. *Neues Jahrbuch für Mineralogie Abhandlungen*, 150, 273-306.
- Boudzoumou, F. (1986). *The West Congo Belt and Its Foreland in the Congo: Relations with the Mayombian: Sedimentology of Protozoic Age Sequences*. Doctoral Thesis, Aix-Marseille University.
- Boudzoumou, F., & Trompette, R. (1988). The West-Congolian Pan-African Belt in Congo (Equatorial Africa); A Polycyclic Base Carried over a Subautochthonous Domain Formed by the Mayombe Aulacogene and the West Congo Basin. *Bulletin of the Geological Society of France*, 4, 889-896. <https://doi.org/10.2113/gssgfbull.IV.6.889>
- Bouénitéla, V. T. T. (2019). *The Paleoproterozoic (Eburnean) Domain of the Mayombe*

- Chain (Congo-Brazzaville): Origin and Tectono-Metamorphic Evolution* (448 p). Thesis, University of Rennes 1.
- Cavalcante, C., Fossen, H., Almeida, R. P. D., Hollanda, M. H. B. M., & Egydio-Silva, M. (2019). Reviewing the Puzzling Intracontinental Termination of the Aracuaí-West Congo Orogenic Belt and Its Implications for Orogenic Development. *Precambrian Research*, 322, 85-98. <https://doi.org/10.1016/j.precamres.2018.12.025>
- Coban, H., & Flower, M. F. (2007). Late Pliocene Lamproites from Bucak, Isparta (South-west Turkey): Implications for Mantle “Wedge” Evolution during Africa-Anatolia Plate Convergence. *Journal of Asian Earth Sciences*, 29, 160-176. <https://doi.org/10.1016/j.jseas.2006.06.006>
- Condie, K. C. (2005). High Field Strength Element Ratios in Archean Basalts: A Window to Evolving Sources of Mantle Plumes? *Lithos*, 79, 491-504.
- Cullers, R. L., & Graf, J. L. (1984). Rare Earth Elements in Igneous Rocks of the Continental Crust: Intermediate and Silicic Rocks—Ore Petrogenesis. In *Developments in Geochemistry* (Vol. 2, pp. 275-316). Elsevier. <https://doi.org/10.1016/B978-0-444-42148-7.50013-7>
- Dadet, P. (1969). *Explanatory Note for the Geological Map of the Republic of Congo Brazzaville at 1:500,000: Area between Parallels 2 and 5 South* (Vol. 70). BRGM Editions.
- Delpomdor, F., Kant, F., Tack, L., & Pr eat, A. (2019). Cyclicity and Sequence Stratigraphy of the Neoproterozoic Uppermost Haut Shiloango-Lukala Carbonate Ramp System in the Lower Congo Region (Democratic Republic of the Congo): Example of Tectonostratigraphic Control versus Climatic Changes. *Journal of African Earth Sciences*, 160, Article 103636. <https://doi.org/10.1016/j.jafrearsci.2019.103636>
- Djama, L. M. (1988). *The Granite Massif of Mfoubou and the Metamorphic Base of Guena (Mayombe Range, Congo)*. Doctoral Dissertation, University Nancy 1.
- Djama, L. M. J., Bazika, U. V. M., Boudzoumou, F., & Mouzeo, K. (2018). Petrology and Geodynamic Context of Metabasic Rocks of Nemba Complex in the West Congo Fold Belt (Republic of Congo). *International Journal of Geosciences*, 9, 1-18. <https://doi.org/10.4236/ijg.2018.91001>
- Djama, L. M., Leterrier, J., & Michard, A. (1992). Pb, Sr and Nd Isotope Study of the Basement of the Mayumbian Belt (Guena Gneisses and Mfoubou Granite, Congo): Implications for Crustal Evolution in Central Africa. *Journal of African Earth Sciences (and the Middle East)*, 14, 227-237. [https://doi.org/10.1016/0899-5362\(92\)90100-Q](https://doi.org/10.1016/0899-5362(92)90100-Q)
- Dussin, I. A., & Dussin, T. M. (1995). Supergrupo Espinhaço: Modelo de evolu o geodin mica. *Geonomos*. <https://doi.org/10.18285/geonomos.v3i1.212>
- Fatehi, H., & Ahmadipour, H. (2018). Geochemistry and Petrogenesis of Metabasites from the Gol-e-Gohar Complex in Southern Sanandaj-Sirjan Metamorphic Zone, South of Iran; Evidences for Crustal Extension and Magmatism at Early Palaeozoic. *Geologica Acta*, 16, 293-319.
- Fitton, J. G., Saunders, A. D., Norry, M. J., Hardarson, B. S., & Taylor, R. N. (1997). Thermal and Chemical Structure of the Iceland Plume. *Earth and Planetary Science Letters*, 153, 197-208. [https://doi.org/10.1016/S0012-821X\(97\)00170-2](https://doi.org/10.1016/S0012-821X(97)00170-2)
- Fram, M. S., & Leshner, C. E. (1993). Geochemical Constraints on Mantle Melting during Creation of the North Atlantic Basin. *Nature*, 363, 712-715.
- Frey, F. A., Weis, D., Borisova, A. Y., & Xu, G. (2002). Involvement of Continental Crust in the Formation of the Cretaceous Kerguelen Plateau: New Perspectives from ODP Leg 120 Sites. *Journal of Petrology*, 43, 1207-1239. <https://doi.org/10.1093/petrology/43.7.1207>

- Frimmel, H. E., Basei, M. S., & Gaucher, C. (2011). Neoproterozoic Geodynamic Evolution of SW-Gondwana: A Southern African Perspective. *International Journal of Earth Sciences*, 100, 323-354. <https://doi.org/10.1007/s00531-010-0571-9>
- Fullgraf, T., Callec, Y., Thiéblemont, D., Gloaguen, E., Charles, N., Le Métour, J., Prian, J.-P., Boudzoumou, F., Delhay-Prat, V., Moreau, F., Kebi-Tsoumou, S., & Ndiele, B. (2015). *Explanatory Note for the Geological Map of the Republic of Congo at 1/200,000, Feuille Dolisie*. Editions BRGM, 342 p.
- Green, T. H. (1994). Experimental Studies of Trace-Element Partitioning Applicable to Igneous Petrogenesis—Sedona 16 Years Later. *Chemical Geology*, 117, 1-36. [https://doi.org/10.1016/0009-2541\(94\)90119-8](https://doi.org/10.1016/0009-2541(94)90119-8)
- Heilbron, M., & Machado, N. (2003). Timing of Terrane Accretion in the Neoproterozoic-Eopaleozoic Ribeira Orogen (SE Brazil). *Precambrian Research*, 125, 87-112. [https://doi.org/10.1016/S0301-9268\(03\)00082-2](https://doi.org/10.1016/S0301-9268(03)00082-2)
- Hirschmann, M. M., Baker, M. B., & Stolper, E. M. (1998). The Effect of Alkalis on the Silica Content of Mantle-Derived Melts. *Geochimica and Cosmochimica Acta*, 62, 883-902. [https://doi.org/10.1016/S0016-7037\(98\)00028-3](https://doi.org/10.1016/S0016-7037(98)00028-3)
- Hossie, G. (1980). *Contribution to the Structural Study of the West-Congolian Chain (Pan-African) in the Congolese Mayombe*. Doctoral Dissertation, University Montpellier 2.
- Jung, S., Hoernes, S., & Mezger, K. (2000). Geochronology and Petrogenesis of Pan-African, syn-Tectonic, S-Type and Post-Tectonic A-Type Granite (Namibia): Melting Products from Crustal Sources, Fractional Crystallization and Entrainment of Surrounding Rocks. *Lithos*, 50, 259-287. [https://doi.org/10.1016/S0024-4937\(99\)00059-6](https://doi.org/10.1016/S0024-4937(99)00059-6)
- Kamgang, P., Chazot, G., Njonfang, E., & Tchoua, F. (2008). Geochemistry and Geochronology of Mafic Rocks from Bamenda Mountains (Cameroon): Source Composition and Crustal Contamination along the Cameroon Volcanic Line. *Comptes Rendus Geoscience*, 340, 850-857. <https://doi.org/10.1016/j.crte.2008.08.008>
- Kampunzu, A. B., & Cailteux, J. (1999). Tectonic Evolution of the Lufilian Arc (Central Africa Copper Belt) during Neoproterozoic Pan African Orogenesis. *Gondwana Research*, 2, 401-421. [https://doi.org/10.1016/S1342-937X\(05\)70279-3](https://doi.org/10.1016/S1342-937X(05)70279-3)
- Le Bayon, B., Callec, Y., Fullgraf, T., Lasseur, E., Thiéblemont, D., Charles, N., Gloaguen, E., Paquet, F., Gouin, J., Giresse, P., Makolobongo, B., Obambi, U., Mouloundou Niangui, E., & Miassouka Mpika, R. (2015). *Explanatory Note for the Geological Map of the Republic of Congo at 1:200,000, Conkouati Sheet*. Éditions BRGM, 242 p.
- Lightfoot, P. C., Hawkesworth, C. J., Devey, C. W., Rogers, N. W., & Calsteren, P. V. (1990). Source and Differentiation of Deccan Trap Lavas: Implications of Geochemical and Mineral Chemical Variations. *Journal of Petrology*, 31, 1165-1200. <https://doi.org/10.1093/petrology/31.5.1165>
- Mahoney, J. J., Sheth, H. C., Chandrasekharam, D., & Peng, Z. X. (2000). Geochemistry of Flood Basalts of the Toranmal Section, Northern Deccan Traps, India: Implications for Regional Deccan Stratigraphy. *Journal of Petrology*, 41, 1099-1120. <https://doi.org/10.1093/petrology/41.7.1099>
- Marques, L. S., Dupré, B., & Piccirillo, E. M. (1999). Mantle Source Compositions of the Paraná Magmatic Province (Southern Brazil): Evidence from Trace Element and Sr-Nd-Pb Isotope Geochemistry. *Journal of Geodynamics*, 28, 439-458. [https://doi.org/10.1016/S0264-3707\(99\)00020-4](https://doi.org/10.1016/S0264-3707(99)00020-4)
- Martins-Neto, M. A. (2000). Tectonics and Sedimentation in a Paleo/Mesoproterozoic Rift-Sag Basin (Espinhaço Basin, Southeastern Brazil). *Precambrian Research*, 103,

- 147-173. [https://doi.org/10.1016/S0301-9268\(00\)00080-2](https://doi.org/10.1016/S0301-9268(00)00080-2)
- Martins-Neto, M. A., Pedrosa-Soares, A. C., & Lima, S. A. D. A. (2001). Tectono-Sedimentary Evolution of Sedimentary Basins from Late Paleoproterozoic to Late Neoproterozoic in the Sao Francisco Craton and Araçuaí Fold Belt, Eastern Brazil. *Sedimentary Geology*, *141*, 343-370. [https://doi.org/10.1016/S0037-0738\(01\)00082-3](https://doi.org/10.1016/S0037-0738(01)00082-3)
- Maurin, J. C. (1993). The West-Congolian Pan-African Chain: Correlation with the East Brazilian Domain and Geodynamic Hypothesis. *Bulletin of the Geological Society of France*, *164*, 51-60.
- Maurin, J. C., Boudzoumou, F., Djama, L. M., Gioan, P., Michard, A., & Mpemba-Boni, J. (1991). The West Congo Proterozoic Chain and Its Foreland in Congo: New Geochronological and Structural Data, Implications in Central Africa. *Proceedings of the Academy of Sciences. Series 2, Mechanics, Physics, Chemistry, Universe Sciences, Earth Sciences*, *312*, 1327-1334.
- McCulloch, M. T., & Gamble, J. A. (1991). Geochemical and Geodynamical Constraints on Subduction Zone Magmatism. *Earth and Planetary Science Letters*, *102*, 358-374. [https://doi.org/10.1016/0012-821X\(91\)90029-H](https://doi.org/10.1016/0012-821X(91)90029-H)
- McDonough, W. F., & Sun, S. S. (1995). The Composition of the Earth. *Chemical Geology*, *120*, 223-253. [https://doi.org/10.1016/0009-2541\(94\)00140-4](https://doi.org/10.1016/0009-2541(94)00140-4)
- Mfere, A. P. A., Delpomdor, F., Proust, J. N., Boudzoumou, F., Callec, Y., & Pr at, A. (2020). Facies and Architecture of the SCIC Formation (Schisto-Calcaire Group), Republic of the Congo, in the Niari-Nyanga and Comba Subbasins of the Neoproterozoic West Congo Basin after the Marinoan Glaciation Event. *Journal of African Earth Sciences*, *166*, Article ID: 103776. <https://doi.org/10.1016/j.jafrearsci.2020.103776>
- Mickala, O. R., Vidal, L., Boudzoumou, F., Affaton, P., Vandamme, D., Borschneck, D., & Miche, H. (2014). Geochemical Characterization of the Marinoan "Cap Carbonate" of the Niari-Nyanga Basin (Central Africa). *Precambrian Research*, *255*, 367-380. <https://doi.org/10.1016/j.precamres.2014.10.001>
- Nagudi, B., Koeberl, C., & Kurat, G. (2003). Petrography and Geochemistry of the Singo Granite, Uganda, and Implications for Its Origin. *Journal of African Earth Sciences*, *36*, 73-87. [https://doi.org/10.1016/S0889-5362\(03\)00014-9](https://doi.org/10.1016/S0889-5362(03)00014-9)
- Nakamura, K. (1977). Volcanoes as Possible Indicators of Tectonic Stress Orientation—Principle and Proposal. *Journal of Volcanology and Geothermal Research*, *2*, 1-16. [https://doi.org/10.1016/0377-0273\(77\)90012-9](https://doi.org/10.1016/0377-0273(77)90012-9)
- Noce, C. M., Pedrosa-Soares, A. C., Da Silva, L. C., Armstrong, R., & Piuzana, D. (2007). Evolution of Polycyclic Basement Complexes in the Araçuaí Orogen, Based on U-Pb SHRIMP Data: Implications for Brazil-Africa Links in Paleoproterozoic Time. *Precambrian Research*, *159*, 60-78. <https://doi.org/10.1016/j.precamres.2007.06.001>
- Nsungani, P. C. (2012). *The Pan-African Chain of North-West Angola: Petrostructural, Geochemical and Geochronological Study*. Doctoral Dissertation, Montpellier 2 University.
- Oliveros, V., Morata, D., Aguirre, L., F eraud, G., & Fornari, M. (2007). Magmatismo asociado a subducci on del Jur sico a Cret cico Inferior en la Cordillera de la Costa del norte de Chile (18°30'-24°S): Geoqu mica y petrogenese. *Revista Geol gica de Chile*, *34*, 209-232. <https://doi.org/10.5027/andgeoV34n2-a03>
- Patel, R., Shankar, R., Sarma, D. S., & Panda, A. (2021). Geochemistry and Petrogenesis of Tholeiitic Dykes from the Chotanagpur Gneissic Complex, Eastern India. *Journal of Earth System Science*, *130*, Article No. 160. <https://doi.org/10.1007/s12040-021-01646-7>

- Pearce, J. A. (1983). Role of the Sub-Continental Lithosphere in Magma Genesis at Active Continental Margins. In C. J. Hawkesworth, & M. J. Norry (Eds.), *Continental Basalts and Mantle Xenoliths* (pp. 230-249). Shiva Cheshire.
- Pearce, J. A. (1996). A User's Guide to Basalt Discrimination Diagrams. In D. A. Wyman (Ed.), *Trace Element Geochemistry of Volcanic Rocks: Applications for Massive Sulphide Exploration* (pp. 79-113). Geological Association of Canada.
- Pearce, J. A. (2008). Geochemical Fingerprinting of Oceanic Basalts with Applications to Ophiolite Classification and the Search for Archean Oceanic Crust. *Lithos*, *100*, 14-48. <https://doi.org/10.1016/j.lithos.2007.06.016>
- Pearce, J. A., & Cann, J. R. (1973). Tectonic Setting of Basic Volcanic Rocks Determined Using Trace Element Analyses. *Earth and Planetary Science Letters*, *19*, 290-300. [https://doi.org/10.1016/0012-821X\(73\)90129-5](https://doi.org/10.1016/0012-821X(73)90129-5)
- Pearce, J. A., & Norry, M. J. (1979). Petrogenetic Implications of Ti, Zr, Y, and Nb Variations in Volcanic Rocks. *Contributions to Mineralogy and Petrology*, *69*, 33-47. <https://doi.org/10.1007/BF00375192>
- Pedrosa-Soares, A. C., Alkmim, F. F., Tack, L., Noce, C. M., Babinski, M., Silva, L. C. D., & Martins-Neto, M. A. (2008). Similarities and Differences between the Brazilian and African Counterparts of the Neoproterozoic Araçuaí-West Congo Orogen. *Geological Society, London, Special Publications*, *294*, 153-172. <https://doi.org/10.1144/SP294.9>
- Pedrosa-Soares, A. C., Cordani, U. G., & Nutman, A. (2000). Constraining the Age of Neoproterozoic Glaciation in Eastern Brazil: First U-Pb (SHRIMP) Data of Detrital Zircons. *Revista Brasileira de Geociências*, *30*, 58-61. <https://doi.org/10.25249/0375-7536.2000301058061>
- Pedrosa-Soares, A. C., De Campos, C. P., Noce, C., Silva, L. C., Novo, T., Roncato, J., & Alkmim, F. (2011). Late Neoproterozoic-Cambrian Granitic Magmatism in the Araçuaí Orogen (Brazil), the Eastern Brazilian Pegmatite Province and Related Mineral Resources. *Geological Society, London, Special Publications*, *350*, 25-51. <https://doi.org/10.1144/SP350.3>
- Pedrosa-Soares, A. C., Vidal, P., Leonardos, O. H., & De Brito Neves, B. B. (1998). Neoproterozoic Oceanic Remnants in Eastern Brazil: Further Evidence and Refutation of an Exclusively Ensialic Evolution for the Araçuaí-West Congo Orogen. *Geology*, *26*, 519-522. [https://doi.org/10.1130/0091-7613\(1998\)026<0519:NORIEB>2.3.CO;2](https://doi.org/10.1130/0091-7613(1998)026<0519:NORIEB>2.3.CO;2)
- Piccirillo, E. M., Melfi, A. J., Comin-Chiaromonti, P., Bellieni, G., Ernesto, M., Marques, L. S., & Stolfa, D. (1988). Continental Flood Volcanism of the Paraná Basin (Brazil). In J. D. Macdougall (Ed.), *Continental Flood Basalts* (pp. 195-238). Springer. https://doi.org/10.1007/978-94-015-7805-9_6
- Piqué, A., Ait Brahim, L., Ait Ouali, R., Amrhar, M., Charroud, M., Gourmelen, C., & Tricart, P. (1998). Structural Evolution of the Atlas Domains of the Maghreb in the Meso-Cenozoic: The Role of Inherited Structures in the Deformation of the Atlas Domain of North Africa. *Bulletin of the Geological Society of France*, *169*, 797-810.
- Rocha-Júnior, E. R., Marques, L. S., Babinski, M., Nardy, A. J., Figueiredo, A. M., & Machado, F. B. (2013). Sr-Nd-Pb Isotopic Constraints on the Nature of the Mantle Sources Involved in the Genesis of the High-Ti Tholeiites from Northern Paraná Continental Flood Basalts (Brazil). *Journal of South American Earth Sciences*, *46*, 9-25. <https://doi.org/10.1016/j.jsames.2013.04.004>
- Rolland, Y., Pecher, A., & Picard, C. (2000). Middle Cretaceous Back-Arc Formation and Arc Evolution along the Asian Margin: The Shyok Suture Zone in Northern Ladakh (NW Himalaya). *Tectonophysics*, *325*, 145-173. [https://doi.org/10.1016/S0040-1951\(00\)00135-9](https://doi.org/10.1016/S0040-1951(00)00135-9)

- Rollinson, H. R. (1996). Tonalite-Trondhjemite-Granodiorite Magmatism and the Genesis of Lewisian Crust during the Archaean. *Geological Society, London, Special Publications*, 112, 25-42. <https://doi.org/10.1144/GSL.SP.1996.112.01.02>
- Ross, P. S., & Bédard, J. H. (2009). Magmatic Affinity of Modern and Ancient Subalkaline Volcanic Rocks Determined from Trace-Element Discriminant Diagrams. *Canadian Journal of Earth Sciences*, 46, 823-839. <https://doi.org/10.1139/E09-054>
- Schandl, E. S., & Gorton, M. P. (2002). Application of High Field Strength Elements to Discriminate Tectonic Settings in VMS Environments. *Economic Geology*, 97, 629-642. <https://doi.org/10.2113/gsecongeo.97.3.629>
- Sun, S. S., & McDonough, W. F. (1989). Chemical and Isotopic Systematics of Oceanic Basalts: Implications for Mantle Composition and Processes. *Geological Society, London, Special Publications*, 42, 313-345. <https://doi.org/10.1144/GSL.SP.1989.042.01.19>
- Tack, L., Wingate, M. T. D., Liégeois, J. P., Fernandez-Alonso, M., & Deblond, A. (2001). Early Neoproterozoic Magmatism (1000-910 Ma) of the Zadinian and Mayumbian Groups (Bas-Congo): Onset of Rodinia Rifting at the Western Edge of the Congo Craton. *Precambrian Research*, 110, 277-306. [https://doi.org/10.1016/S0301-9268\(01\)00192-9](https://doi.org/10.1016/S0301-9268(01)00192-9)
- Talbi, F., Jaafari, M., & Tlig, S. (2005). Neogene Magmatism of Northern Tunisia: Petrogenesis and Geodynamic Events. *Revista de la Sociedad Geológica d'España*, 18, 241-252.
- Teixeira, W., & Figueiredo, M. C. H. (1991). An Outline of Early Proterozoic Crustal Evolution in the São Francisco Craton, Brazil: A Review. *Precambrian Research*, 53, 1-22. [https://doi.org/10.1016/0301-9268\(91\)90003-S](https://doi.org/10.1016/0301-9268(91)90003-S)
- Thiéblemont, D., Callec, Y., Fernandez-Alonso, M., & Chène, F. (2018). A Geological and Isotopic Framework of Precambrian Terrains in Western Central Africa: An Introduction. In S. Siegesmund, M. Basei, P. Oyhantçabal, & S. Oriolo (Eds.), *Geology of South-west Gondwana* (pp. 107-132). Springer. https://doi.org/10.1007/978-3-319-68920-3_5
- Thiéblemont, D., Chèvremont, P., Castaing, C., Triboulet, C., & Feybesse, J. L. (1994). Geotectonic Discrimination of Basic Magmatic Rocks by Trace Elements. Re-Evaluation Based on a Database and Application to the Pan-African Chain of Togo. *Geodinamica Acta*, 7, 139-157. <https://doi.org/10.1080/09853111.1994.11105264>
- Trompette, R. (2000). Gondwana Evolution; Its Assembly at Around 600 Ma. *Comptes Rendus de l'Académie des Sciences-Series IIA-Earth and Planetary Science*, 330, 305-315. [https://doi.org/10.1016/S1251-8050\(00\)00125-7](https://doi.org/10.1016/S1251-8050(00)00125-7)
- Uhlein, A., Trompette, R. R., & Egydio-Silva, M. (1998). Proterozoic Rifting and Closure, SE Border of the São Francisco Craton, Brazil. *Journal of South American Earth Sciences*, 11, 191-203. [https://doi.org/10.1016/S0895-9811\(98\)00010-8](https://doi.org/10.1016/S0895-9811(98)00010-8)
- Vellutini, P., Rocci, G., Vicat, J. P., & Gioan, P. (1983). Identification of Ophiolitic Complexes in the Mayombe Chain (Gabon-Angola) and New Geotectonic Interpretation. *Precambrian Research*, 22, 1-21. [https://doi.org/10.1016/0301-9268\(83\)90056-6](https://doi.org/10.1016/0301-9268(83)90056-6)
- Vicat, J. P., & Pouclet, A. (2000). Palaeo- and Neoproterozoic Granitoids and Rhyolites from the West Congolian Belt (Gabon, Congo, Cabinda, North Angola): Chemical Composition and Geotectonic Implications. *Journal of African Earth Sciences*, 31, 597-617. [https://doi.org/10.1016/S0899-5362\(00\)80009-3](https://doi.org/10.1016/S0899-5362(00)80009-3)
- Vicat, J. P., & Vellutini, P. (1987). On the Oceanic Origin of Metabasites from the Mayombe Chain (Gabon, Congo, Zaire, Angola). *Precambrian Research*, 36, 163-175. [https://doi.org/10.1016/0301-9268\(87\)90087-8](https://doi.org/10.1016/0301-9268(87)90087-8)

- Wang, Y., Fan, W., Sun, M., Liang, X., Zhang, Y., & Peng, T. (2007). Geochronological, Geochemical and Geothermal Constraints on Petrogenesis of the Indosinian Peralkaline Granites in the South China Block: A Case Study in the Hunan Province. *Lithos*, *96*, 475-502. <https://doi.org/10.1016/j.lithos.2006.11.010>
- Wilson, M. (Ed.) (1989). *Pétrogénèse Ignée*. Springer Pays-Bas.
- Winchester, J. A., & Floyd, P. A. (1977). Geochemical Discrimination of Different Magma Series and Their Differentiation Products Using Immobile Elements. *Chemical Geology*, *20*, 325-343. [https://doi.org/10.1016/0009-2541\(77\)90057-2](https://doi.org/10.1016/0009-2541(77)90057-2)
- Wooden, J. L., Czamanske, G. K., Fedorenko, V. A., Arndt, N. T., Chauvel, C., Bouse, R. M., & Siems, D. F. (1993). Isotopic and Trace-Element Constraints on Mantle and Crustal Contributions to Siberian Continental Flood Basalts, Noril'sk Area, Siberia. *Geochimica and Cosmochimica Acta*, *57*, 3677-3704. [https://doi.org/10.1016/0016-7037\(93\)90149-Q](https://doi.org/10.1016/0016-7037(93)90149-Q)
- Xia, L. Q., & Li, X. M. (2019). Basalt Geochemistry as a Diagnostic Indicator of Tectonic Setting. *Gondwana Research*, *65*, 43-67. <https://doi.org/10.1016/j.gr.2018.08.006>